ACS OMEGA

Open Access

http://pubs.acs.org/journal/acsodf

Review

Cost Effective Photothermal Materials Selection for Direct Solar-Driven Evaporation

Husam Eltigani,* Viriyah Chobaomsup, and Yuttanant Boonyongmaneerat*

Cite This: *ACS Omega* 2024, 9, 27872−27887

Read Online

ACCESS | Metrics & More | Article Recommendations | Supporting Information

ABSTRACT: The cornerstone of eco-friendly and affordable freshwater generation lies in harnessing solar energy for water evaporation. This process involves extracting vapor from liquid water using solar energy. Numerous innovative, low-cost materials have been proposed for this purpose. These materials aim to enable highly controllable and efficient conversion of solar energy into thermal energy while maintaining high cost-effectiveness. Here, in this review paper, we outline the advancements in solar-driven evaporation technology with a focus on optimizing synthesis methods and materials cost. It prioritizes refining evaporation efficiency and affordability using inventive manufacturing methods. By utilizing innovative reasonably priced materials, this process not only ensures efficient resource utilization but also fosters technological advancements in renewable energy applications. Moreover, the affordability of these materials makes solar-powered water evaporation accessible to a wider range of communities, empowering them to address water scarcity challenges.

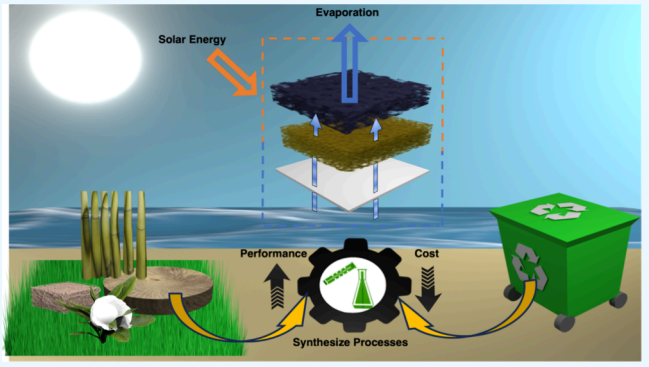

1. INTRODUCTION

The United Nations anticipates a concerning future where five billion people will deal with severe water shortages by 2025.[1,2] It is crucial to implement solutions such as solar desalination systems, especially for rural areas around the world and for various uses like farming and industry. Despite sunlight being renewable, there is an urgent need for low-cost and efficient solar desalination systems from affordable materials, rather than relying on high-cost materials or constructing costly plants for seawater desalination, which can exceed one billion US dollars.[3] Within this framework, photothermal materials emerge in this field of solar evaporation.[4] Photothermal materials can offer portability and cost-effectiveness since they can be constructed using easily accessible materials[5] and efficiently converting sunlight into heat.

Numerous materials have been investigated as photothermal candidates for solar-driven evaporation, including plasmonic nanoparticles such as gold and silver,[6,7] carbonaceous materials like graphene and graphene oxide, carbon black (CB), caron nanotubes (CNTs), transition metal oxides such as titanium dioxide[8] and iron oxide,[9] metal−organic frameworks (MOFs),[10,11] and semiconductors like silicon[12] and copper oxide.[13] Among all, carbonaceous materials exhibit variations in light absorption rates from 500 to 800 nm, with carbon black (CB) materials covering a wide range from 250 to 2500 nm. These variations are attributed to the presence of surface groups and π-conjugated structures in their carbon cores.[14] Notably, graphene exhibits exceptional light absorption capabilities, absorbing 2.3% of light across a wide spectrum due to its unique electronic structure known as "Dirac cones."[15,16] For comparison, plasmonic localized heating occurs when these nanomaterials absorb light, leading to the conversion of light energy into heat via plasmonic oscillations of free electrons.[16,17] Similarly, in semiconductor materials, nonradiative relaxation takes place as absorbed photons generate electron−hole pairs, with the excess energy dissipating as heat through nonradiative pathways instead of being emitted as light.[18] In contrast, thermal vibration in molecules, observed in carbonaceous and organic polymer materials, is triggered by the absorption of light energy, prompting the atoms within the molecules to vibrate and produce heat due to frictional forces.[19] However, despite the advancements in light-to-heat conversion of plasmonic and semiconductors materials with superior electronic properties, they are still primarily studied on a laboratory scale. Their limitations become apparent when considering scaling up solar-driven evaporation processes, leading to high-cost fabrication. For instance, as photothermal materials, plasmonic-active filter paper as a photothermal material can cost about $247 per m^2.[20] Moreover, in terms of cost in kilogram,

Received: March 29, 2024
Revised: June 7, 2024
Accepted: June 10, 2024
Published: June 20, 2024

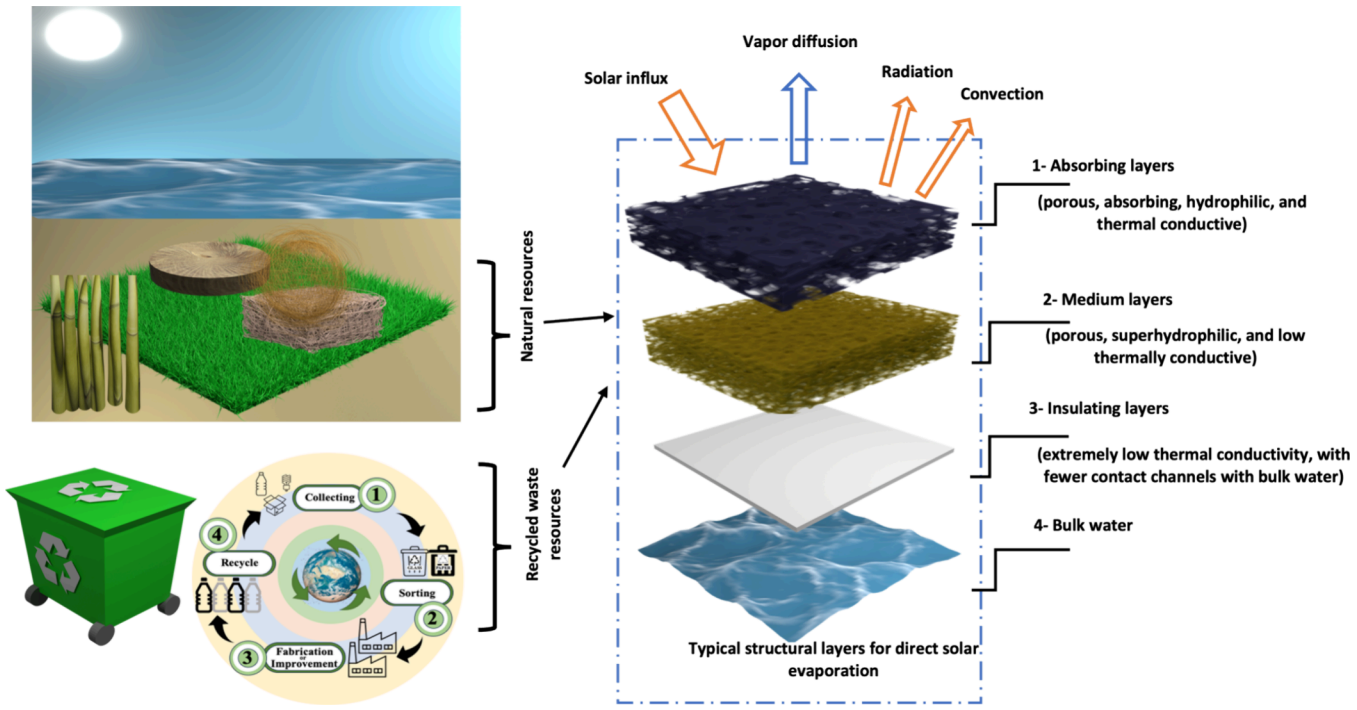

Figure 1. Some abundant fundamental resources of materials, recycling process, and the typical system structure of a solar evaporation system.

plasmonic particles like silver can cost over 500 USD per kg, while semiconductor materials such as TiO_2 are comparatively cheaper, at less than 50 USD per kilogram.[21] In comparison, copper is notably cheaper than conventional noble metals and exhibits a wide plasmonic absorption spectrum.[22]

Materials capable of absorbing a broad solar spectrum can be further combined with low-cost materials as composites. For example, gold nanoparticles can be decorated onto a natural wood matrix (Basswood) to produce plasmonic wood using Sn^{2+} to reduce Ag^{+} or Au^{3+}[23] or via deep metallization of the cell wall on Balsa wood (Ochroma pyramidale, porosity (90%)). This method can deal with the limited diffusion of mass and rapid reduction of metal ions by accurate removal of constituents from the cell wall, resulting in better accessibility using NaOH treatment.[24] In another example, the integration of titanium nitride (TiN) and hydrophilic semireduced graphene oxide (semi-rGO) composites is feasible using methods like in situ microwave reduction to enable this integration. TiN nanoparticles enhance solar photon absorption and hydrophilicity while reducing heat loss.[25] However, the precise control of the nanoparticle ratio is paramount to obtain good performance such as in the case of gold/silver ratio as each nanoparticle can absorb specific wavelengths within the light spectrum.[26] Furthermore, the effectiveness of such plasmonic-based absorbing materials in photothermal conversion heavily hinges on the careful design of their nanoparticle arrangements.[27,28]

In this paper, we emphasize the cost-effectiveness factor, which is limited in the literature. Here, we focus on both affordable materials such as wood, bamboo, various biomass materials, polymers, and carbonaceous materials, along with evaporation rates, providing cost-effectiveness calculations, while also highlighting the related synthesis processes. We fully agree with researchers who have expressed their recommendation that cost and scalability are crucial in the development of this field of solar-driven evaporation.[29−31] Moreover, our goal is also to address that the essence of cost-effectiveness lies in optimizing resource allocation to achieve maximum efficiency and value. Therefore, this paper serves as a roadmap in the development of performance through materials selection and encourages the use of low-cost materials in the field of solar-driven evaporation. Eventually, it can open a new avenue for aiding in scaling up solar-driven evaporation for more practical applications, addressing the world's urgent need for affordable seawater desalination solutions.

2. SOLAR STEAM GENERATION VIA LOCALIZED HEATING

Thermal concentration and localized heating[32] enable achievement of solar evaporation. So solar evaporators must possess qualities such as strong high absorption, high thermal conductivity for large energy conversion at solid−liquid interface, porosity and wettability for transportation water from bulk of water to the sun-exposed surface area, and the ability to deal with salt accumulation that can hinder the evaporation rate along with cost-effectiveness. Figure 1 shows typical system layers and the most common abundant resources of materials for solar-driven evaporation. In solar evaporator systems, the functionality of the top layers is typically to enhance solar absorption and generate a hot region for evaporation.[33] Meanwhile, the medium layers with superhydrophilicity and interconnected channels ensure rapid, continuous water pumping by leveraging capillary force, while their low thermal conductivity provides excellent heat insulation.[34,35] Lastly, the objective of the bottom layers is to restrict the transfer of generated heat to the underlying water body.[36]

However, for optimal performance and achieving high salt rejection, various approaches can be considered. One such approach involves combining different structures to create multiple resonances, resulting in broadband optical characteristics.[37] For rapid water supply, nanofibrous materials

https://doi.org/10.1021/acsomega.4c03040
ACS Omega 2024, 9, 27872−27887

produced through electrospinning technique exhibit favorable characteristics, including suitable pore size, increased specific surface area, enhanced porosity, interconnected pores, and adjustable fiber diameter, all of which contribute to improving continuous water supply.[38] Another approach, through the combination of pores with different diameters and hydrophilic pores, creates multilevel water channels with internal gaps and microchannels, facilitating efficient water supply and continuous steam flow.[39]

To tackle salt accumulation, one example approach involves the rediffusion of salt back into the bulk brine. This can be achieved through vaporization enthalpy recycling using a multistage configuration. Solar absorption and interfacial heating facilitate evaporation on opposite sides, while vertically aligned layers reduce heat loss. This solution, costing only \$1.54 m^{-2} for the materials, boasts a high efficiency of 385% and an evaporation rate of 5.78 (L m^{-2} h^{-1}).[40] Furthermore, certain researchers are embracing the biomimetic approaches inspired by nature,[41,42] such as the mangrove plant (Avicennia marina) and its leaf structure, to address salt management issues. This innovative strategy is crucial as rising seawater salinity poses a significant threat to aquatic ecosystems. By utilizing low-cost superhydrophilic nanostructured chemically etched titanium meshes in a scalable mangrove-mimicked device, researchers have observed that the crystallized salt exhibits porosity and hydrophilicity. The precipitation patterns are intricately linked to the salt concentration distribution across the evaporator surface. Specifically, a higher supersaturation at the edge induces a greater chemical potential difference of salt, thus lowering the energy hurdle for salt nucleation.[43]

3. COST-EFFECTIVENESS

Cost-effectiveness emerges as a critical factor in the design of a solar evaporation system, as it establishes a direct connection between the cost of materials and the evaporation rate, calculated by dividing the evaporation rate by the cost of the materials. Therefore, achieving high evaporation rate performance becomes paramount in enhancing cost-effectiveness, as it effectively offsets the expenses associated with materials. Figure 2 shows a schematic depicting the interconnection between cost-effectiveness, evaporation performance, and materials cost and solar irradiation. In this case solar irradiation influences a high evaporation rate, while materials cost is influenced by factors such as abundance, accessibility, usability, and intrinsic properties (ease of fabrication and absence of costly treatments). Additionally, sourcing low-cost materials from natural resources, recycled materials, waste materials, with favorable structural combinations of composite materials can significantly contribute to the affordability and efficiency of solar-driven evaporators. This approach not only allows for the utilization of readily available resources in the surrounding environment but also presents opportunities to enhance existing designs by replacing materials or techniques. Moreover, incorporating these cost-effective materials into solar evaporator production processes with simple manufacturing techniques[44] further enhances accessibility and usability, resulting in practical and affordable desalination materials that also minimize waste materials pollution.[45] However, it has to be mentioned here that the availability of resources and the threshold for cost-effectiveness typically rise and fall together, with a greater suitability for the use of waste natural resources and recycled materials. Figure 3 compares the cost, abundance, and performance of various materials based on their sources.

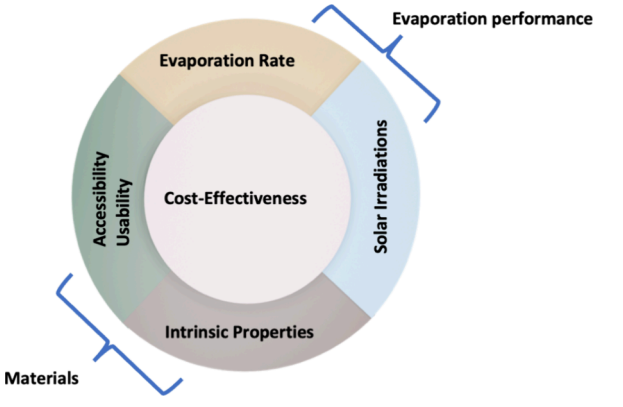

Figure 2. A schematic depicting the interconnection between cost-effectiveness, evaporation performance, solar irradiation, and the affordable properties of materials.

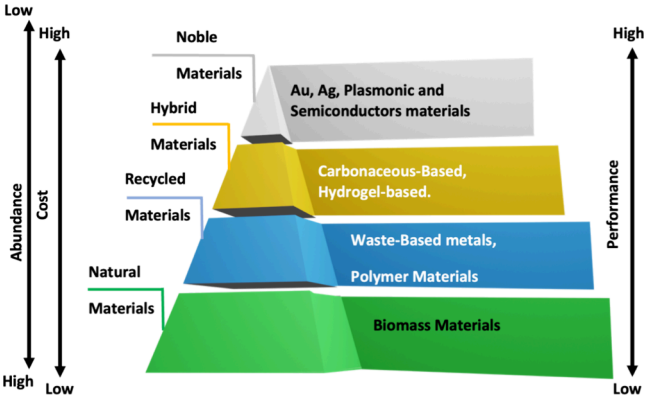

Figure 3. Materials hierarchy for solar-driven applications, from noble materials to natural materials, with arrows indicating the balance between cost, performance, and abundance.

The cost effectiveness ϵ (g h^{-1} $\$^{-1}$) can be defined by the equation:[46]

$$\epsilon = r/c \times 1000 \quad (1)$$

where r refers to the evaporation rate (kg m^{-2} h^{-1}) and c is the cost of raw materials (\$ m^{-2}).

Most of the synthesis approaches for fruits, as an example, involve both carbonization with freezing and drying process. Carbonization increases solar absorption by boosting the carbon concentration, but it necessitates high temperatures, typically ranging from 300 to 700 °C.[47] However, cost-effective methods exist, such as hydrothermal carbonization, which can be conducted at lower temperatures ranging from 150 to 190 °C. These processes can take as little as 20 to 40 min.[48,49] It is more promising that hydrothermal carbonization to produce biochar products from such garden and park wastes is being further developed to enhance its economic viability by maximizing heat recovery through the recycling of process water,[50] as illustrated in Figure 4. Moreover, even handmade strategy treatments such as crochet, as shown in Figure 5, can be considered an economical approach to produce, for instance, a cost-effective handmade flowerlike light absorber (HFLA) with a superhydrophilic surface, especially after processes such as the dyeing of waste materials.[51]

https://doi.org/10.1021/acsomega.4c03040
ACS Omega 2024, 9, 27872−27887

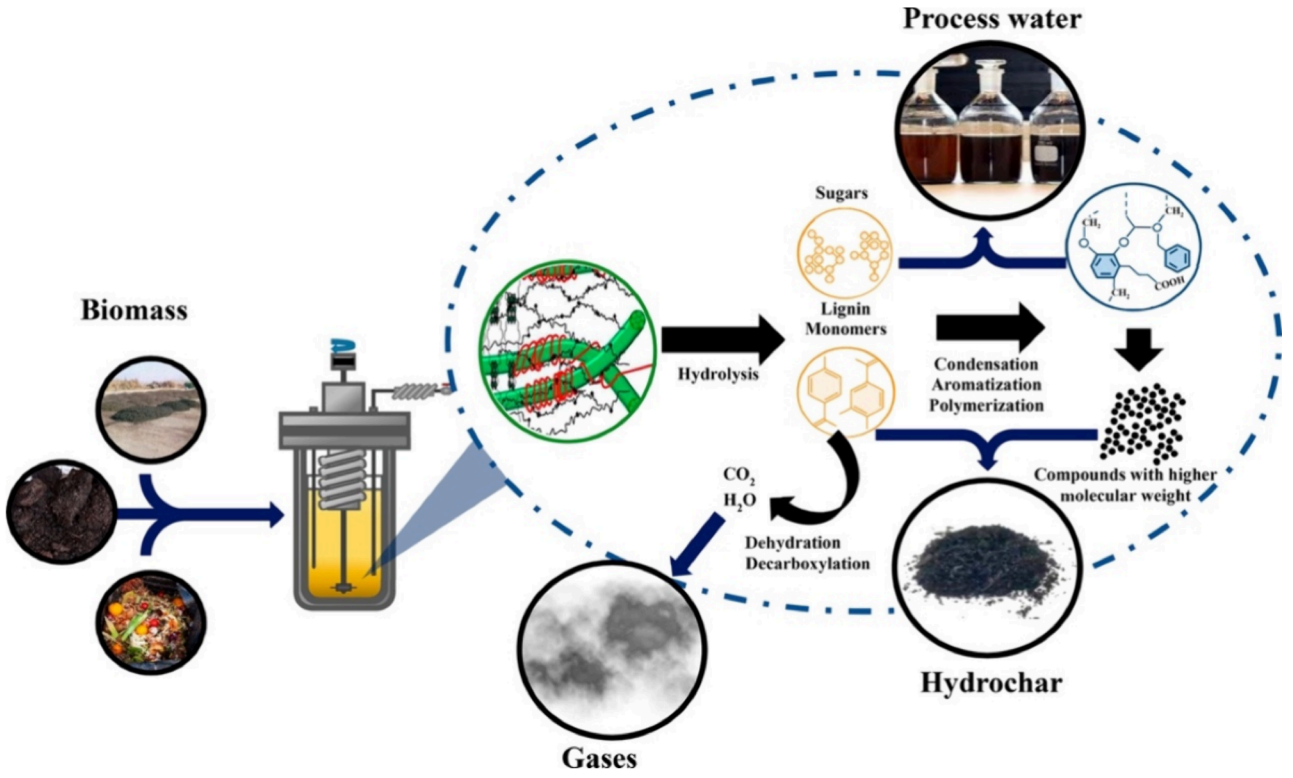

Figure 4. Fundamental pathways of reaction in hydrothermal carbonization. Reproduced from Ipiales et al.[50] Copyright 2024 American Chemical Society.

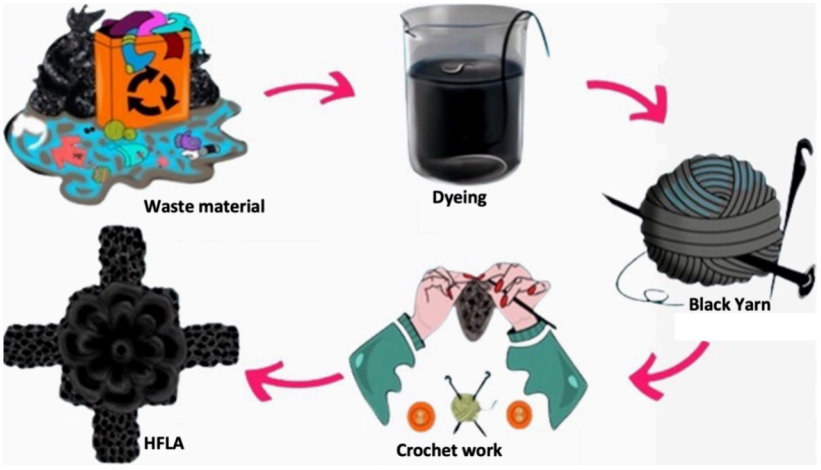

Figure 5. Knitting route of handmade flowerlike light absorber (HFLA) from waste material or black yarn. Adapted from Javed et al.[51] Copyright 2021 American Chemical Society.

For post-treatment cost such as drying, the annualized investment cost C_a for the dryers, that can be used for synthesizing of fruits, can be approximated by employing the parameters detailed in the equation:

$$C_a = C_{ac} + C_m - V_{as} + C_e \quad (2)$$

where V_{as} [USD] and C_{ac} [USD] are the salvage values of the dryers and annualized capital cost, respectively. C_m [USD] is the annual maintenance costs, and C_e [USD] refers to the annual cost of energy (electricity) required for the drying process.[49]

4. BIOMASS MATERIALS

4.1. Wood, Bamboo. Generally, wood displays high hydrophilicity because its cell walls are composed of fibers containing hydroxyl groups ((because hydroxyl groups form hydrogen bonds with water))[52] derived from lignin, cellulose, and hemicellulose[53] as shown in Figure 6. Additionally, wood exhibits low thermal conductivity, ranging from approximately 0.2 to 0.45 W m^{-1} K^{-1},[54] making it suitable for water transportation with low heat loss.[55,56] Wood contains two types of channels with varying diameters: large vessels and small tracheids. Continuous water transport is made possible by these channels facilitating the process.[57] Besides, that wood, which showed reduced lumen size following treatment, also

https://doi.org/10.1021/acsomega.4c03040
ACS Omega 2024, 9, 27872−27887

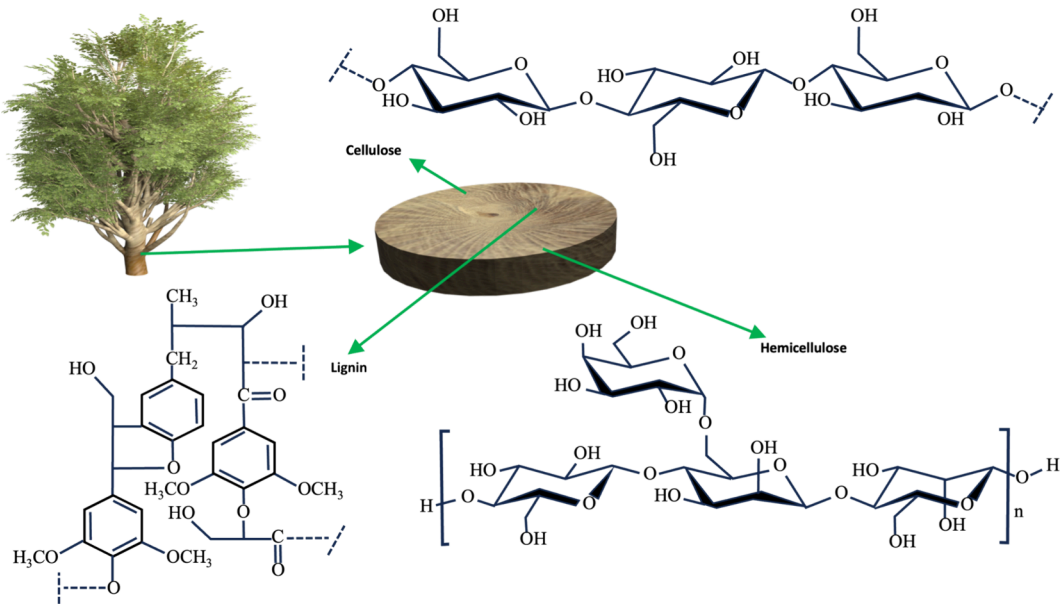

Figure 6. Chemical structures of cellulose, lignin, and hemicellulose of wood.

prompted the generation of interfacial water (IW) and water clusters. These lumens in the wood were utilized for water absorption in the alignment direction.[58,59] In addition, a varied range of porosity is found in natural woods, determined by their density as shown in the study by Jia et al.[60] They illustrated different densities (and consequently, porosities) ranging from approximately 180 kg m^{-3} in Basla trees to around 1500 kg m^{-3} in Cocobolo trees.

Engineering wood with hierarchical microchannels is feasible by such as assembling the lumens of wood cells with poly(vinyl alcohol) (PVA) through the ice-templating approach. It is worth mentioning that the vertically aligned lumens of wood cells have diameters ranging from several tens to hundreds of micrometers,[61] Using this approach also of ice templating is regarded also as environmentally friendly, readily available, inexpensive, and nontoxic,[62] nevertheless there are still numerous constraints within the freezing method of ice-templating approach, such as the organization of structural design.[63] Treatment of wood surface can serve as a way to enhance solar steam generation and as a sustainable source of materials. For example, Poplar (Populus) trees (their leaves that vary from rounded to triangular shape) are utilized as photothermal materials. When their wood are coated with a gold nanolayer (approximately 50 nm thick) through sputter coating, this process results in establishing a solar evaporator reaching an evaporation rate of 4.02 (kg m^{-2} h^{-1}) under 3 sun irradiance. In this work, high-porosity wood was chosen because it leads to robust capillary action, resulting in a lower likelihood of pore fouling and impurities settling on the surface.[64] Additionally, by carbonization, the cost of producing a carbon layer is much lower with an area of 1 m^2 and a thickness of 4 mm reported at approximately $0.12, while the cost of wood is around $0.078 per 1 m^2 area and 1 mm thickness, based on prices in China.[65] However, additional efforts are required to control the thickness and achieve a low-cost carbon layer on the surface.

A new direction to confine energy to the light-absorbing layer was pursued by Xie et al. They constructed a conical three-dimensional (3D) flexible wooden evaporator with a materials cost of only $0.12 per square meter. This evaporator exhibited highly efficient evaporation performance, reaching up to 1.79 (kg m^{-2} h^{-1}), about 1.6 times higher than that of the 2D evaporator with a stable evaporation rate for 30 days. This improvement was attributed to a larger evaporation area and reduced scattering of light. They achieved this using wood as a substrate and a tannic acid complex as the light-absorbing material (wavelength range of 200−800 nm). Additionally, the delignification process also made the wood increasingly hydrophilic.[66] With inspiration from differences in wood morphology, Zhang et al. engineered wood lumens via p-toluenesulfonic acid (p-TsOH)-assisted hydrothermal treatment to improve solar-to-thermal efficiency. After treatment, wood lumens became more hydrophilic due to a decrease in diameter from 40−60 μm to 10−20 μm. The material cost was estimated to be about $3.3 per square meter, with good performance indicated by an efficiency of 87% and an evaporation rate of 2.2 kg m^{-2} h^{-1} and good stability, as there was no apparent change noticed after a duration of 18 days.[67] Remarkably, the flamed-straw evaporator, fabricated by Zhang et al., makes use of the unused agricultural residue of corn straw. Their design demonstrates a rapid evaporation rate of 1.497 (kg m^{-2} h^{-1}), as average for a five-cycle test, featuring a double-layer flamed straw configuration. The design represents a typical solar-driven interfacial evaporator with ultralow thermal conductivity (0.042 W m^{-1} K^{-1}) and an efficient water supply, all achieved with materials costing only $0.8 per square meter. The low hermal conductivity (0.042 W m^{-1} K^{-1}) along the growth direction significantly enhances its thermal insulation capabilities. Additionally, it possesses an internal porous structure and the capability to float autonomously and provides consistent functionality for producing solar vapor over prolonged durations.[68] Interestingly, Zhu et al. employed two wood-based layers (less than one USA dollar per meter squared) to address salt accumulation and found that the bilayer wood remained operational for 100 h under 5 sun in seawater. Notably, salt deposition only became evident at illumination intensities of ≥5 sun, indicating that at higher intensities, surface-evaporated water could not be promptly replenished by the water refilling the channels. Importantly, salt accumulation is not a concern

https://doi.org/10.1021/acsomega.4c03040
ACS Omega 2024, 9, 27872−27887

under ambient solar irradiation (1 sun) because slower evaporation rates at lower intensities hinder salt crystallization. Furthermore, the bilayer wood possesses a unique self-regenerating ability: precipitated salt within the wood structure rapidly dissolves or falls back into the surrounding seawater, depending on its solubility, during nighttime.[69]

Table 1 presents noteworthy above examples of wood processing along with their corresponding performance and cost-effectiveness, showcasing various sequences and variations of synthesis procedures. These examples may be beneficial in leading to accurate predictions of outcomes, as they will help develop more favorable properties and, ultimately, optimize costs.

Bamboo, another natural resource, is often hailed as a giant woody grass and has garnered significant attention for its abundance, renewability, porous structure, inherent hydrophilicity, and relatively affordable price. Moreover, its surface can be treated with various materials, making it suitable for applications such as solar evaporation.[70,71] For example, silver microspheres doped in bamboo shoot porous carbon (Ag-BSC) can enhance the evaporation rate (ER) and efficiency to 1.51 (kg m^{-2} h^{-1}) and 86.8%, respectively. The surface wettability of bamboo shoot improves at a pyrolysis temperature of 750 °C, where cellulose, hemicellulose, and lignin in bamboo shoots are pyrolyzed into tar, carbon dioxide, and other substances. (Pyrolysis is a method where organic substances like biomass are heated without oxygen present.) Additionally, the porous arrangement of bamboo shoot porous-carbon (BSC) enables a beneficial distribution pattern for Ag nanoparticles (Ag NPs). The resulting cost-effectiveness of AC-BS is 34000 (g h^{-1} $\$^{-1}$).[72] In another instance, a study conducted by Li et al., regarding bamboo charcoal (BC), presents notable advantages. BC features broad light absorption and an arched, porous structure, mechanical properties with costs not exceeding $1 per square meter. Its efficiency reaches 84% under 1 sun radiation, and it boasts an evaporation rate of approximately 1.191 (kg m^{-2} h^{-1}) under the same conditions. Moreover, it meets the requirements for water transport, and its synthesis is straightforward through cutting, sawing, and carbonization methods (in an atmosphere furnace (VBF−1200X)), and nitrogen gas was introduced. The temperature was increased to 1000 °C at a rate of 5 °C per minute for a duration of 2 h. Importantly, BC's sustainability is evident in its ability to maintain hydrophilicity (measured contact angles of 29.7° and 25.3°) attributed to its chemical components as observed in FTIR spectra (C−N)/(H−N−H)/(O−H).[73]

4.2. Fruits and Vegetables. Efforts are being made to incorporate organic waste such as fruit and vegetable waste into the synthesis of solar evaporators.[74] These materials are typically considered readily available or cost-free, though expenses may arise from incorporating additional metal components during the preparation process. For example, graphite combined with coconut fibers as a hybrid system can cost approximately US$4.86 per kilogram, based on the component costs per kilogram produced, as outlined by Ovando-Medina and coauthors.[75] These costs break down as follows: graphite = 0.033, coconut fibers and recycled polystyrene (including its drying, grinding, and transportation) = 1.0, solvents = 3.33, and processing = 0.5). This properly combined system can offer an effective area of 1.73 m^2 and can achieve an evaporation rate of 1.73 ± 0.007 (kg m^{-2} h^{-1})

Table 1. Highlighting the Synthesis Sequences of Some Wood-Based Materials with Their Evaporation Performance and Cost-Effectiveness

Evaporator	Efficiency, evaporation rate, estimation cost, cost-effectiveness, and sunlight intensity	Main synthetic sequences
Delignified wood (DW)-TA-Fe^3 (3D, cone shape)[66]	90%, 1.79 (kg m^{-2} h^{-1}), $0.12 m^{-2}, 14916.67 (g h^{-1} $\$^{-1}$), 1 kW m^{-2}	Main raw material: Wood Veneers (90 mm × 90 mm × 0.55 mm (tangential × longitudinal × radial)); synthesis sequences: immersing (solution of 2.5 M NaOH and 0.4 M Na_2SO_3, 100 °C, 7 h), resining (in boiling water), result: (delignified wood DW), immersing (DW in a 4% w/v tannic acid TA, 12 h), dipping [(DW-TA) in 4% w/v $Fe_2S_3O_{12}$ aqueous solution, 2 h], result (DW-TA-Fe^3)
Carbonized wood (R-CW)), flat shape[67]	87%, 2.2 (kg m^{-2} h^{-1}), ~$3.3 m^{-2}, 666.67 (g h^{-1} $\$^{-1}$), 1 kW m^{-2}	Main raw material: a bulk wood prepared from basswood (3 cm × 1.5 cm × 1.5 cm); synthesis sequences: immersing (in a hydrothermal autoclave containing a water solution of p-toluene sulfonic acid (70% w/w, 30 mL), heating (at 100 °C, 140 or 180 °C for 8 h), result (a carbonized wood (R-CW)), rising (three times with water (100 mL) at room temperature), freezing and drying
Flamed straw (cylindrical shape)[68]	86%, 1.497 (kg m^{-2} h^{-1}), $0.8 m^{-2}, 1871.25 (g h^{-1} $\$^{-1}$), 1 kW m^{-2}	Main raw material: corn straw (3 cm × 1.3 cm × 0.2 cm); synthesis sequences: peeling (peeling of the block of the corn straw), immersing (in DI-water to remove the impurities), freezing and drying (24 h to get porous structure), heating (on an alcohol burner for five second to carbonize the top surface), quenching (rapidly quenching in cold water for 60 s), result (flamed straw 13 mm, comprising a layer for absorbing light (3 mm) and a layer for pumping water (17 mm))
Bilayer wood (flat shape)[69]	~99%, 11.2 (kg m^{-2} h^{-1}), <$1 m^{-2} 11200 (g h^{-1} $\$^{-1}$), 1 kW m^{-2}	Main raw material: basswood (4.5 cm × 4.5 cm × 2.9 cm); synthesis sequences: cutting (A wood log was cut perpendicular to the wood growth direction to form wood blocks (4.4 cm × 4.5 cm)), pressing and carbonizing (on a hot plate at 500 °C for 30 s to carbonize the top surface), result (carbonized layer with ≈3 mm thick), polishing (with 2000 grit sandpaper)

https://doi.org/10.1021/acsomega.4c03040
ACS Omega 2024, 9, 27872−27887

under only 1.2 W m^{-2} of illumination, demonstrating an excellent efficiency of 91.5%.

The biochar material, collected from agricultural waste such as coconut husk and rice husk, and modified with cryptomelane, as presented in a work by Zhang and coauthors, offers an affordable option. This results in an evaporation rate of 1.247 (kg m^{-2} h^{-1}) and a photothermal conversion efficiency of 89.36% under 1 sun (1 kW/m^2). The process of biochar involved in this case includes drying, pyrolyzing, and pulverizing before being ground into powder. This method proves to be a valuable approach for enhancing the efficiency of photothermal conversion using cryptomelane manganese (potential active adsorption sites can be generated after the modification of cryptomelane, and more light energy can be converted into heat). To mention here, the pyrolysis method, conducted with minimal or no oxygen, allows for the production of cost-effective biochar (BC) from materials like rice husks and straws. This results in biochar with increased surface area and enhanced porous structures.[76] A cheap biomass material, such as daikon (costing 3 US$ m^{-2}) reported by Zhu et al., can be carbonized, leading to in a honeycomb cellular structure with numerous excellent hydrophilic properties due to interconnected channels and closely packed pores. These features act as photon traps, allowing for solar absorption of more than 95.5% and an evaporation rate of 1.57 (kg m^{-2} h^{-1}). The process involves freeze-drying before the carbonization process in a nitrogen atmosphere. The thin film of carbonized daikon can be supported by polystyrene (PS) foam as an insulator with a low cost of USD 4.234 per square meter.[77] Another notable example is mushroom, which can be utilized for efficient solar steam generation. After undergoing a soaking treatment for softening, it can be straightforwardly carbonized at 500 °C in an argon atmosphere, leading to an impressive evaporation rate of 1.5 (kg m^{-2} h^{-1}).[78] Furthermore, the ultrablack carbon black-coated pomelo peel (UB-PP) presents an affordable option (high light absorption and high emissivity). The UB-PP evaporator achieves a high evaporation rate of 1.81 (kg m^{-2} h^{-1}) thanks to its distinctive multicurvature gradient and interconnected porous structure with an overall cost as low as $2.7 per square meter, offering significant cost-effectiveness 670.37 (g h^{-1} $\$^{-1}$).[79]

4.3. Other Biomass Materials. Photothermal nanoparticles derived from a natural abundant biomass have a wide range of investigation to use in the solar evaporation system due to their intrinsic properties such as algae, dead leaves, and green moss.[80,81] It was reported that green moss has open-microgrooves, which can supply adequate water to the evaporation surface, while its open capillary channels can reject the precipitated salt.[82] Additionally, its ability to anchor itself to various surfaces, like rocks and trees surfaces, is what makes it readily accessible in outdoor environments as it is flourishing amidst the rugged landscapes of rocky areas.

A compelling advancement by Luo et al., involves the incorporation of a readily available biomass, Nicandra physalodes (Linn.) Gaertn. polysaccharide, into a poly(vinyl alcohol) matrix, resulting in the creation of a cost-effective hybrid hydrogel solar evaporator. This innovative approach yields an impressive evaporation rate of 3.51 (kg m^{-2} h^{-1}) when exposed to sunlight. The reported material cost for implementing this system is approximately $7.95 per square meter.[83] Another example and at a cost of under $1 per square meter, Gao and his team[84] employed cotton and affordable candle soot to create a solar evaporator. They achieved this by applying the candle soot onto one side of cotton fabric, resulting in a self-floating Janus solar absorber boasting high efficiency and an evaporation rate of 86.3%, and 1.375 (kg m^{-2} h^{-1}), respectively, under solar irradiation of 1 kW m^{-2}. This approach is notably economical as it necessitates no specialized equipment. The round cotton fabric, measuring 5 cm in diameter, was moistened with water before being placed in proximity to a candle flame for various durations to collect candle soot. In another case, involving the use of cotton, Gao et al.[85] explored a promising method for mitigating salt accumulation: vapor generation was directed downward through the fabric's backside, employing Janus fabric crafted from recycled cotton textiles. To achieve this, they applied a carbon black @silicone photothermal slurry to the fabric's upper surface after prewetting treatment. This approach effectively curtailed excessive penetration to the underside of the fabric while ensuring strong adhesion. The resulting fabrication boasted an impressive evaporation rate of 1.17 (kg m^{-2} h^{-1}) and an efficiency rating of 77.8%, all achieved at a low cost of USD 4.234 per m^2. Cotton fabric was chosen as the substrate due to its exceptional hydrophilicity and widespread availability, while the silicone's sealing properties endowed the Janus fabric with directional vapor permeability. Furthermore, in a study conducted by Wang et al.,[86] the collaborative influence of the photothermal membrane and the cattail leaf-based water transporter led to the complete cattail leaf-derived solar evaporator achieving an evaporation rate of 1.46 (kg m^{-2} h^{-1}), along with a solar thermal efficiency of 87.48% under 1-solar (1 kW m^{-2}) irradiation. To mention, the cattail leaf (CL) is abundant in carbon, lignin, and cellulose, making it suitable for crafting mats, cushions, and various household items and, most importantly, here as part for fabricating a solar evaporator. In another study, Flour powder, obtained by grinding raw grains and beans, was utilized by Yang et al., in the production of Carbon Bread for solar evaporation. The synthesis technique is simple and highly technologically advanced, involving the mixing of flour with yeast, water, and carbon black, outcoming in dough, an elastic substance capable of scaling up. This dough demonstrates impressive performance metrics: an evaporation rate of 1.28 (kg m^{-2} h^{-1}), efficiency of 85.9%, and a cost of $0.84 per meter square. Most notably, it achieves high cost-effectiveness, 1505.88 ($g.h^{-1}.\$^{-1}$) as a result of (1.28 kg m^{-2} h^{-1}/$0.84 m^{-2}) multiplied by 1000. The dough displayed both elasticity and strength, a 3D cross-linking network structure, accompanied by a porous structure (nanometer-sized pores of approximately 7−20 nm and micron-sized pores of approximately 10−500 μm). This porousness is primarily attributed to the formation of disulfide bonds between gliadin and glutenin proteins, as well as the bonding of starch and proteins present in the flour.[87] Table 2 illustrates different biomass material processing methods, highlighting their performance, cost-effectiveness, and diverse synthesis procedures.

5. POLYMER MATERIALS

5.1. Recycled Polymer. It has been reported that the quantity and weight of small plastic particles on the ocean's surface layer from 1979 to 2019 are around 82−358 trillion plastic particles, totaling a weight ranging from 1.1−4.9 million tonnes according to current global estimation[88] and over 10 million tonnes of polyethylene terephthalate (PET) added to the annual plastic waste.[89] However, through extraction,

https://doi.org/10.1021/acsomega.4c03040
ACS Omega 2024, 9, 27872−27887

Table 2. Highlighting the Synthesis Sequences of Some Biomass Materials with Their Evaporation Performance and Cost-Effectiveness

Evaporator	Efficiency, evaporation rate, estimation cost, cost-effectiveness, and sunlight intensity	Main synthetic sequences
Ultrablack pomelo peel[79]	93.43%, 1.81 (kg m^{-2} h^{-1}), $2.7 m^{-2}, 670.37 g h^{-1} $\$^{-1}$, 1 kW m^{-2}	Main raw materials: Pomelo peel from fresh Shatian pomelo; synthesis sequences: coating (with solution contains carbon black mass concentration of 25% in the epoxy resin), drying, curing (in an oven 60 °C, 24 h), curing (again in an oven, temperature 120 °C, 2 h), result (ultrablack pomelo peel (UB-PP))
Soot-deposited Janus fabrics[84]	86.3%, 1.375 (kg m^{-2} h^{-1}), <1$ m^{-2}, 1375 g h^{-1} $\$^{-1}$, 1 kW m^{-2}	Main raw materials: circular cotton fabric (diameter of 5 cm), a candle; synthesis sequences: wetting (with water), exposing (exposed to candle flame for different times to capture candle soot), result (self-floating Janus cotton fabric)
Carbonized cattail leaf (CCL)[86]	87.48%, 1.46 (kg m^{-2} h^{-1}), $3.1 m^{-2}, 470.97 g h^{-1} $\$^{-1}$, 1 kW m^{-2}	Main raw materials: cattail leaf; synthesis sequences: washing (2 g of cattail leaf), carbonizing (in a tube furnace and maintained in an nitrogen atmosphere (about 20 mL per minute) at a heating rate of 5 °C min^{-1} to 700 °C for 2 h), immersing (in 30 mL of 1 M HCl for 1 h), rising (DI-water), drying under a vacuum, and result (0.3 g CCL)
Carbon bread[87] (cuboid shape)	~85.9%, 1.28 (kg m^{-2} h^{-1}), $0.85 m^{-2}, 1505.88 g h^{-1} $\$^{-1}$, 1 kW m^{-2}	Main raw materials: flour (30.0 g), carbon black particles (0.075 g), yeast (0.5 g); synthesis sequences: mixing (combining flour, carbon black particles and yeast in 17 mL distilled water (30 °C) with siring), kneading (thoroughly kneading until resulting in a smooth and elastic dough), foaming (sealing the dough and letting it foam in an oven at 30 °C for two hours), transferring and foaming (transferring the dough into a mold and allowing it to foam again at 30 °C for 1 h), baking (baking the dough in an oven at 150 °C for 30 min), and cutting (transforming the as-prepared carbon bread into a cuboid shape with dimensions of 10 mm by 10 mm and a thickness of 20 mm)

purification, and recycling, their use as solar evaporators can be enabled.

Interestingly, a solar evaporator made from plastic achieves a peak evaporation rate of 2.49 kg m^{-2} h^{-1}, demonstrating an impressive efficiency of 90.8%. However, more modification is required to obtain hydrophilic behavior to adjust the intrinsic hydrophobic behavior, for example, through base-catalyzed trans-esterification with polyols.[90] A film blend consisting of recycled carbon soot and poly(vinyl alcohol) can absorb sunlight in a wide range of wavelengths, and its particles can be fixed with hydrophilic polymeric poly(vinyl alcohol) (PVA), to form a porous network promoting in conversion energy 95.1%.[91] Another example, from lithium-ion battery waste, a graphite porous hydrogel (RG-PH) can be efficiently recycled and created using cross-linking foaming technology, leading to a solar evaporator with a high evaporation rate of 3.4278 (kg m^{-2} h^{-1}) even under a single solar irradiation.[92] Also, a low-cost ~$2 per meter square of light polyethylene terephthalate (PET) cloths with good capillary action can serve as a high-efficiency solar steam generator, and the cost can reach ~$10 m^{-2} for expanded polyethylene (EPE) foam.[93]

A pulp-natural rubber foam (PNR) was utilized by Zhang et al.,[94] through a straightforward surface carbonization procedure to produce carbonized pulp-natural rubber foam (CPNR) with cost-effectiveness (338.9 g h^{-1} $\$^{-1}$ of total materials). This evaporator achieved an evaporation rate of 1.62 kg per square meter per hour and an evaporation efficiency of 98.09% under 1 sun illumination. Figure 7 exhibits the surface carbonization treatment, nano/microporous network structures of both (PNR) and (CPNR) with a schematic of the light absorption and trapping within the framework of the foams. The hydroxyl groups present in the CPNR foam evaporator enhance the concentration of heat and aid in its ability to absorb and pump water effectively. Although, there are different kinds of evaporators, however, mostly they typically have nano/micro for absorption of the light and water transportation. In another example, Wang and his team[95] reported on the development of a bionic fabric structure, inspired by the aquatic plant pistia, with the goal of reducing heat loss and maximizing material efficiency. The manufacturing process, which includes blended yarn spinning and multibeam weaving, is easily scalable for mass production. Furthermore, a unique loop-pile fabric (LPF) has been created, utilizing double-helix carbon yarn (DCY), to enable indirect contact between the photothermal layer and bulk water. With a low raw material cost of USD 3.54 per meter and under 1 sun illumination, the water evaporation reached 1.50 kg per square meter per hour, and efficiency reached 88.70%. Notably, in another approach, through a traditional weaving machine, hydrophilic ultrafine denier polypropylene fiber and expandable polyethylene foam strips, with water-repellent properties, were used by Li et al.,[96] as an solar evaporator with high cost-effectiveness around 1700 (g h^{-1} $\$^{-1}$), and evaporation rate 1.408 (kg m^{-2} h^{-1}) and an efficiency of 92.43%. This rapid evaporation is facilitated by the careful arrangement of micro- and macro-capillary channels through the adjustment of the wrap yarn density. These channels enable continuous water transport and can act as drainage pathways for high salinity water, driven by the Marangoni effect caused by temperature differences varying along the water in the yarns.

5.2. Polymer Composite. Polymer composite materials add another option in the synthesis of a cheap solar evaporator. One of the most effective combinations in low-cost evaporator

https://doi.org/10.1021/acsomega.4c03040
ACS Omega 2024, 9, 27872−27887

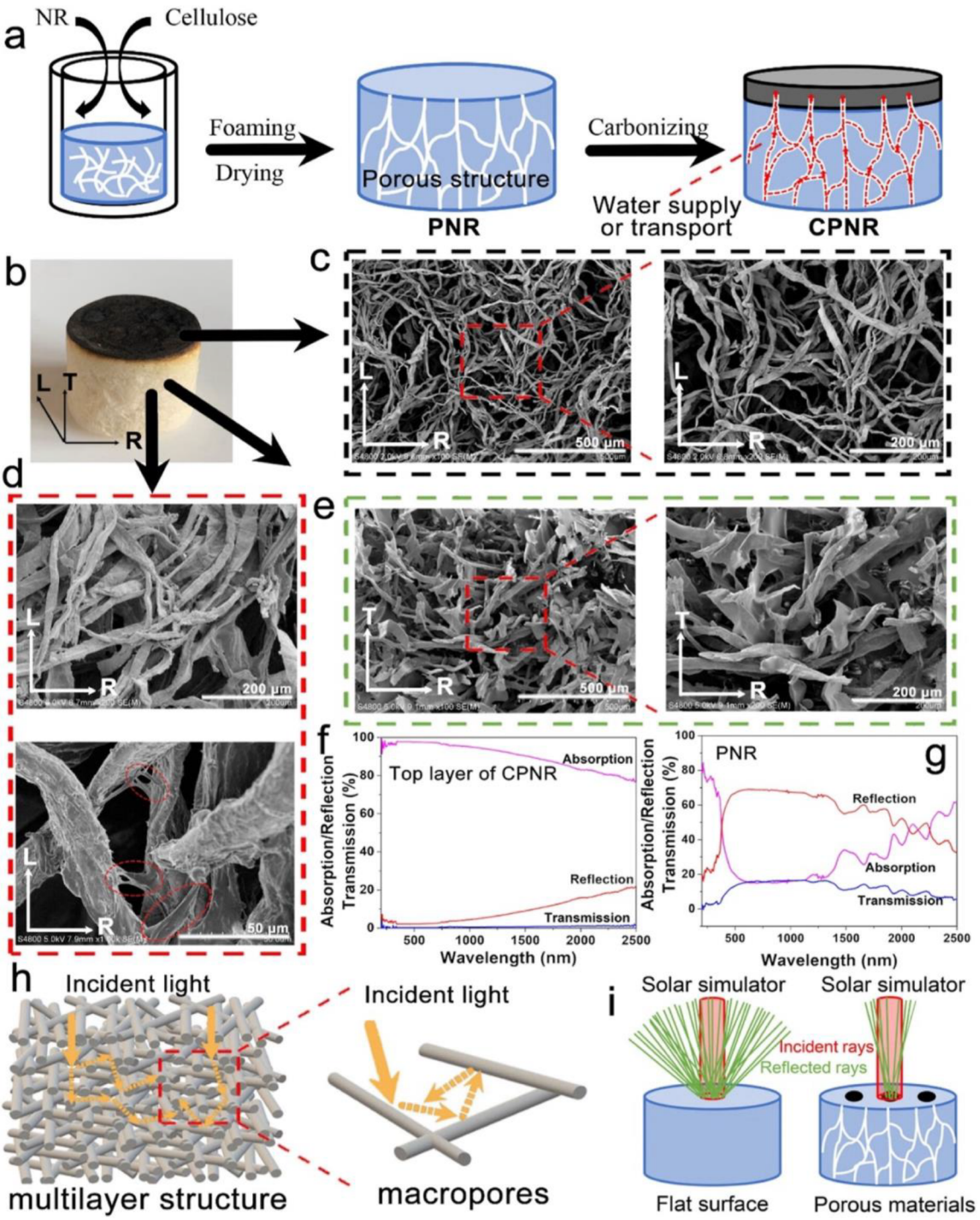

Figure 7. (a) Diagram showing the synthesis process of CPNR foam evaporator. (b) Digital photo of CPNR foam evaporator; SEM images of porous CPNR foam (c) and PNR foam (d) at varying magnifications. (e) Cross-sectional SEM image unveiling porous structure of PNR foam. Spectra illustrating absorption, reflection, and transmission for CPNR foam evaporator (f) and PNR foam (g). (h) Diagram illustrating the capture of incident light within the foam network structure. (i) Diagram showing reflection of incident light on flat and porous foam surfaces. Reproduced from Zhang et al.[94] Copyright 2023 American Chemical Society.

structures with only a one-step method is achieved using cheap semiconductor materials such copper oxide (CuO), which has a small bandgap of 1.2 eV, combined with porous ionic polymer (PIP), emeraldine salt (ES) form of polyaniline (PANI), along with reduced graphene oxide. The synthesis is achieved by the oxidative polymerization of aniline monomer by ammonium peroxydisulfate in an acidic medium, yielding a solar evaporator with evaporation rate of 2.02 (kg m^{-2} h^{-1}) and an efficiency of 94.2%.[97] In another case, carbon cloth (4 × 10 cm^2) can be used to serve as the substrate with vertically oriented graphene (VGs) growing on it via plasma-enhanced chemical vapor deposition (PECVD). Paraffin wax and nickel foil are used to prevent leakage. This fabricated evaporator, with U-shape, achieved an evaporation rate of 0.70 (kg m^{-2}

https://doi.org/10.1021/acsomega.4c03040
ACS Omega 2024, 9, 27872−27887

h^{-1}) and an energy efficiency of 46.5% under dark conditions, producing 855 L of potable water at an estimated cost of $11.2 per cubic meter. However, under a light intensity of 1 kW m^{-2}, it reached a high evaporation rate of 1.36 (kg m^{-2} h^{-1})—nearly double that of dark conditions—along with a solar-vapor energy efficiency of 90.0%.[98] Another example of nontoxic rebus and cheaper combination is geopolymer−mesoporous carbon composites (GBMCC) leading to a record high water vapor generation rate of 7.55 (kg m^{-2} h^{-1}). The total estimated cost for a single GBMCC device, which includes 3.62 g of geopolymer and 1.8 g of BMC, is just $0.0273. However, for large-scale production, the cost is estimated to be only $39 per square meter. This is due to the low price of carbon materials at $0.0147 per gram, which is considerably cheaper than graphene oxide (GO) at $26.5 per gram and Ti_2O_3 at $4.65 per gram.[99] Another approch, the fabrication process of composite polymers can be achieved with a single-step calcination process. For example, melamine foam can be synthesized as a solar evaporator by calcination process. This foam, made from a copolymer of formaldehyde and melamine-sodium bisulfite, possesses ideal traits like an interconnected structure and high porosity. Most importantly, it is lightweight and costs approximately $2−3 per square meter for its materials and yeilding a good performance with an an efficiency of 87.3% under 1 W m^{-2} and an evaporation rate of 1.270 kg m^{-2} h^{-1}.[100]

5.3. Hydrogel-Based Materials. A hydrogel is a three-dimensional cross-linked polymeric network[101] and has captured increasing attention among researchers investigating the field of solar-driven water. Importantly, solar evaporator platforms using aerogel for the production of pure water can be manufactured at a cost below $1 per kilogram.[102] The hydrogel film efficiently can capture and reuse the thermal radiation energy making it well-suited for salt-resistance strategies.[103] However, the practical use of a hydrogel evaporator is challenging due to its instability and complicated preparation process, but some approaches with controllable regulation have emerged, such as 3D black hydrogel evaporator Fe-PTPU with cost effectiveness (43.8 g h^{-1} $\$^{-1}$) and high evaporation rate 2.65 (kg m^{-2} h^{-1}). The process started by using a mixture of ethanol and water as the solvent for polyvinyl alcohol (PVA) and tannic acid (TA), the ethanol was subsequently evaporated to form a hydrogel directly on the polyurethane (PU) sponge skeleton. Besides that, the black chelate formed by TA with Fe^{3+} could endow the sponge with a photothermal conversion layer. The sponge provides porosity and stability to the overall structure.[104]

Another example of a synthesis method, through a simple fabrication process using lignin nanoparticles (NPs) and cellulose nanofibers (CNFs); a light-absorbing porous hydrogel (LAPH) can be fabricated to improve both $\pi-\pi$ stacking and light-absorbing property and serves as hydrophilic support. The evaporator's performance can achieve an evaporation rate 3.17 (kg m^{-2} h^{-1}) and a solar steam generation efficiency of 83.4% under 1 sun irradiation.[105] In another approach, a bilayer aerogel consisting of PPy/cellulose can prepared through the in situ formation of PPy on the top layer of cellulose hydrogel in the presence of phytic acid (PA), followed by freeze-drying. This setup enabled a high evaporation rate of 1.42 (kg m^{-2} h^{-1}), an energy efficiency of 97.8% under 1 sun illumination. However, based on a lab-scale experiment, the materials cost of the aerogel amounts to about $25.1 per square meter, corresponding to a cost-effectiveness of (56.6 g h^{-1} $\$^{-1}$).[106]

Using a different strategy, hydrogel biomimics the natural plant structures, such as mushrooms. It must be mentioned here that mushrooms are well-known for their unique structure, featuring a wide black pileus and a fibrous stipe, which facilitate efficient water circulation. The fibrous stipe ensures rapid water supply to the pileus, while its porous nature acts as a pathway for water transport and establishes a boundary for heat transfer within the water transport layer, minimizing heat loss. The skeleton structure of hydrogels prepared by chemical cross-linking results in a mushroom-structured hydrogel evaporator based on lotus root starch (LR) and poly(vinyl alcohol) (PVA) (PLBH) in self-floating hydrogels, leading to an extraordinary evaporation rate of 3.78 kg m^{-2} h^{-1} under 1 kW m^{-2} with cost-effectives around 358.94 (g h^{-1} $\$^{-1}$).[107] Unlike the previous process, hydrogel foams with closed-cell structures can be created using a controlled foaming and gelation technique ("sol−foaming−gel" strategy) reaching a high cost-effectiveness of 2692 (g h^{-1} $\$^{-1}$) under 1 sun with an evaporation rate of 2.12 (kg m^{-2} h^{-1}). The synthesis process of this work, starting by mixing sodium alginate with surfactants (poly(vinyl alcohol), PVA) to obtain a hydrogel, then stirring to form liquid foam, and spraying HCl solution (1 wt %) onto each foam to initiate cross-linking reactions.[108] Another example by using hydrogel reported by Guo et al.,[109] in their work, the use of materials such as an iron-based metal−organic framework (MOF) and konjac glucomannan (KGM) can incorporate into a poly(vinyl alcohol) (PVA) network. This integration lead to the formation of a low-cost hybrid hydrogel evaporator (HHE) with a high evaporation rate 3.2 (kg m^{-2} h^{-1}) under 1 sun, at a cost of $14.9 per square meter. The affordable biomass, KGM, improves the hydration capability of hydrogels for water activation and offers numerous hydroxyl groups, which facilitate the formation of hydrogen and chelating bonds to efficiently eliminate contaminants. In another case, the use of hydrophilic polyethylene glycol (PEG-4000) hydrogel is reported as the most suitable phase change material (PCM). It should be noted that waste heat, which is not utilized in water vaporization, can be stored by PCM and released for evaporation during nighttime. Moreover, a combination of graphene/cotton sponge coated with a polyethylene glycol (PEG) layer as a PCM, constructed by simply stretching cotton to achieve gradient vertical microchannels, served as a versatile photothermal platform with a high evaporation rate of 2.49 (kg m^{-2} h^{-1}), and high efficiency of 100%.[110]

6. CARBONOUS MATERIALS

Alternative developments in solar-driven evaporation include the utilization of inexpensive materials, such as carbon-based hybrid materials[111] with nanoparticles and metal oxides,[112] as well as the adoption of straightforward fabrication processes and passive solar concentration techniques to enhance efficiency without added complexity. Mostly, carbonous materials exhibit promising results, especially in improving hydrophilicity, cyclability, high absorption capacity of sunlight, and mechanical properties.

Such as graphene doped with nitrogen, as studied by Deng et al.,[113] to enhance hydrophilicity with robust mechanical framework, this enhancement is evident in the superwetting behavior, cost-effectiveness of 1871.25 (g h^{-1} $\$^{-1}$), and excellent thermal insulation of nitrogen-doped graphene

https://doi.org/10.1021/acsomega.4c03040
ACS Omega 2024, 9, 27872−27887

Table 3. Highlighting the Synthesis Sequences of Some Materials with Their Evaporation Performance and Cost-Effectiveness

Evaporator	Efficiency; evaporation rate, cycle; estimation cost; cost-effectiveness; and Sun light intensity	Main synthetic sequences
Nitrogen-doped graphene aeroge (NGA) (cylindrical shape)[113]	86%, 1.497 (kg m^{-2} h^{-1}), \$0.828 m^{-2}, 1871.25 (g h^{-1} $\$^{-1}$), 1 W m^{-2}	Main raw materials: graphene oxide (GO), ethylenediamine (EDA) as source of nitrogen (diameter 2 cm, height 2 cm); synthesis sequences: mixing (GO with EDA at 120 °C for 12 h), result (graphene hydrogel GH), dialysis (GH with 20% ethanol for 6 h), lyophilization to obtain graphene aerogel, annealing (in an argon atmosphere 200−1000 °C), graphitic N, pyridinic N, pyrrolic N, and result (nitrogen-doped graphene aerogel, NGA)
CNTs and DE combined aerogel[116]	91%, 1.67 (kg $m^{-2}h^{-}$), 10 \$6.67 m^{-2}, 250.37 (g h^{-1} $\$^{-1}$), 1 kW m^{-2}	Main raw materials: diatomite (DE), carbon nanotubes (CNTs), aerogel (dimensions 20 × 20 × 3 mm^3); synthesis sequences: DE and acidified CNTs were combined using a freeze-drying technique, with agar powder serving as a gel agent to create the desired aerogel, purified DE and acidified CNTs were dispersed in agar solution at 80 °C, cooling to room temperature, agar was mixed with DE and CNTs and allowed to solidify, it formed a hydrogel, the DE was dispersed throughout the aerogel matrix during the production process
C carbonized nonwoven material[118]	91%, 1.67 (kg m^{-2} h^{-1}), \$1.01 m^{-2}, 250.37 (g h^{-1} $\$^{-1}$), 1 kW m^{-2}	Main raw materials: 6 g toner, nonwoven fabric with a radius of 5 cm; synthesis sequences: mixing (6 g toner with 500 mL water and 20 mL of acetic acid in a beaker), sonication (an ultrasonic vibrator 5 to 10 min), submerging (putting the nonwoven fabric in the beaker that contains toner and the acetic acid), sonication (of the beaker for 10 min), and drying (into a drying box to dry for half an hour)
(CF-ACB)[121]	91.8%, 1.7 (kg m^{-2} h^{-1}), 10 \$1.38 m^{-2}, 1231.88 (g h^{-1} $\$^{-1}$), 1 kW m^{-2}	Main raw materials: ceramic fiber (CF) (a small square of 3 cm × 3 cm), carbon black (CB), polytetrafluoroethylene (PTFE); synthesis sequences: mixing (CB powder with PTFE (60% wt), to form a paste before smearing onto the CF), same thing to add activated carbon AC powder, the composite had an equal mass ratio of AC to CB, with a ratio of 1:1
VAAFs@CDs (cylindrical shape)[122]	93.9%, 2.6 (kg m^{-2} h^{-1}), \$15.01 m^{-2}, 173.21 (g h^{-1} $\$^{-1}$), 1 W m^{-2}	Main raw materials: vertically aligned acetate fibers (VAAFs), (diameter ∼0.8 cm, height 2.5 cm); synthesis sequences: preparing carbon dots (CDs) following the procedure in a reference,[123] dispersing (dispersing the as-prepared CDs' powder in absolute ethyl alcohol), sonication (for 15 min in room temperature to obtain the solution of 20 g/L concentration), dripping (1 mL of CD's ethanol solution to be dripped uniformly on the top surface of saturated VAAFs), and drying (into a drying oven and heated at 60 °C for removing water to obtain VAAFs@CDs)

aerogel (NGA), which promote fluid flow to the surface during solar steam generation. The persisting superwetting property of NGA for weeks in air is attributed to the preferential adsorption of water molecules to the nitrogen-doped sites. Specifically, pyridinic nitrogen acts as the primary adsorption center for water molecules, while the graphitic nitrogen in the graphene layer provides a relatively polarized surface with high affinity against water, extending beyond its own atomic dimensions. In addition, this adaptation of nitrogen with graphene leads to a strong mechanical structure, tested by uniaxial quasi-static compression; stress−strain curves almost remain unchanged for 10 cycles, exhibiting fully reversible compressibility with strain up to 90%, showing a high strength-to-weight ratio of up to ∼6000 (m^{-2} s^{-2}). However, the effect of N-doping on the wettability of carbon-based aerogels requires further study.

In more approaches, Yin et al.[114] proposed a method to enhance cyclic stability by introducing a newly developed double-layer solar absorber. This absorber consists of activated carbon−carbon black composite photothermal materials embedded in a ceramic fiber supporting matrix. The evaporation rate increased significantly to 1.70 (kg m^{-2} h^{-1}) under 1 sun, and the solar-to-vapor energy conversion efficiency reached 91.8% due to improved heat insulation and water pumping mechanisms. The materials used were cost-effective, with a total cost of \$6.67 m^{-2}. Ceramic fiber was chosen as the supporting matrix for its affordability and suitability. The double-layer design facilitated heat insulation, confining the generated heat to the upper layer. In this configuration, the upper carbon layer absorbed light and converted it into heat, while the lower supporting layer provided insulation and facilitated water pumping. In an economic approach, a piece of plasma-activated carbon cloth (ACC), measuring 32.25 cm^2, was utilized by Nguyen et al., as a solar evaporator, with an approximate cost of 1 USD. The affordability of carbon cloth allows for the preparation of large black pieces, with a diagonal length reaching up to 56.5 cm. Carbon fibers allow for abundant intermediate waters that lower the enthalpy for evaporation, yielding an evaporation rate of 1.78 (kg m^{-2} h^{-1}) under 1 sun irradiation that reached nearly double to 3.82 (kg m^{-2} h^{-1}) with a tailored 5 cm-height column shape. The synthesis method including loading the carbon cloth into a low-vacuum plasma chamber was subjected to a 3 min air plasma activation process. The original carbon cloth was initially hydrophobic, with a contact angle of approximately 137°, before the plasma treatment, which caused it to exhibit superhydrophilic behavior.[115]

For improving the light absorption capacity, a natural mineral, diatomite (DE) is employed by Li and his team[116] due to its large number of micropores arranged in an orderly manner inside, lightweight, strong adsorption capacity, and stable chemical properties, and it has a wide source of raw materials and low cost, however, with exhibited excellent combination with carbon nanotube and aerogel (excellent hydrophilicity) with cost-effectiveness around 250.37 (g h^{-1} $\$^{-1}$). DE has a 67% light absorption capacity, and the composite aerogel after the addition of carbon nanotubes CNT shows absorption capacity over 95%. Most interestingly that the CNT/DE aerogel takes only 30 s to reach a temperature of 70.7 °C under 1 sun intensity, which is 33 °C higher than that of DE aerogel. It has to be mentioned here that nanotube ((one-dimensional and possesses a unique and highly ordered atomic and electronic structure within their tubes)) absorption

https://doi.org/10.1021/acsomega.4c03040
ACS Omega 2024, 9, 27872−27887

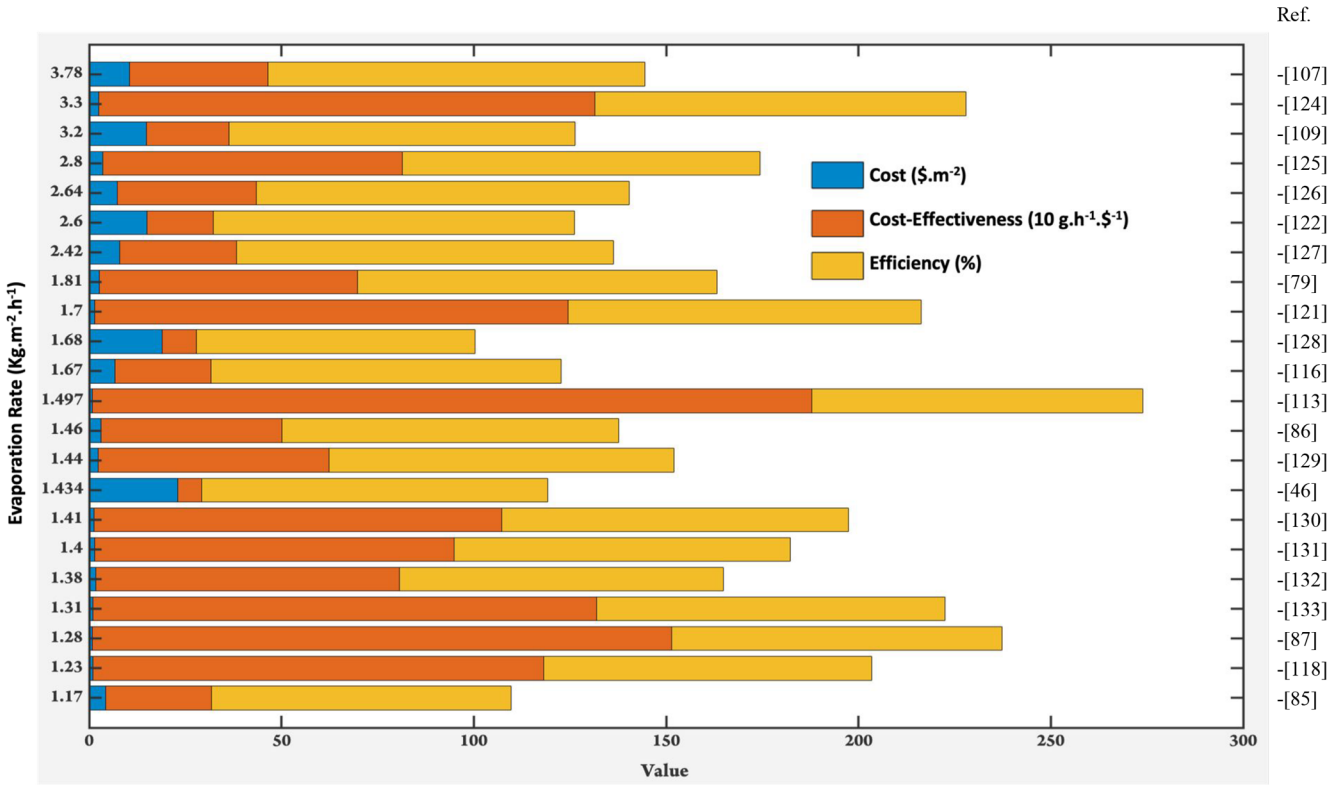

Figure 8. A bullet chart illustrating the cost-effectiveness, evaporation rate, and cost of various solar evaporators.

results from electron shifts between the valence (v) and conduction (c) bands.[117] Moreover, Lv et al., utilize the fibrous arrangement and exceptional absorbency of carbonized nonwoven material ($1.01 m^{-2}). The system involves utilizing carbonized paper (CP) affixed to polystyrene foam to prevent the evaporation material from sinking into the water. CP, derived from low-cost nonwovens through carbonization, boasts high absorbency because of its fibrous composition and offers the benefits of softness and excellent endothermic properties. In their experiments, the evaporation rate achieved with only black cotton was 0.85 (kg m^{-2} h^{-1}), whereas with CP, it reached 1.23 (kg m^{-2} h^{-1}) with high cost-effectiveness 1171.42 (g h^{-1} $\$^{-1}$).[118]

An alternative method to improve light absorbance involves employing an antisalt-fouling materials combination. Salt accumulation can impede both light intensity and the continuous supply of water. For tackling this challenge of salt accumulation, Zhao and his team[119] created a 3D spiral sponge made of gradient graphene (GG) and has cost-effectiveness around 122.52 (g h^{-1} $\$^{-1}$), using environmentally friendly techniques involving spraying coating, air drying, and solar reduction. This 3D network structure enhanced energy recovery and achieved an evaporation rate of 6.5 kg m^{-1} h^{-1} under 1 sun illumination, with the evaporator remaining stable for approximately 72 h. The sponge features a varied graphene network with pore sizes ranging from 150 to 20 μm, facilitating radial brine transport and guiding salt crystallization in specific directions by creating a variance in capillary force across the gradient of pore sizes. Continuous vapor production improves radial brine flow, resulting in the concentration of brine on the outer surface of the GG sponge, thus achieving full separation of water and salt from a brine solution containing 20 wt % salt. In another approach, a study by Zhou et al.,[120] using carbon dots with vertically aligned acetate fibers VAAF derived from a cigarette filter before applying the ethanol solution of CDs onto their upper surface (VAAFs@CDs), demonstrates the spontaneous rejection of salt accumulation through rapid fluid convection within the evaporating interfaces. This system also maintains efficient heat localization while possessing salt-rejection capabilities for long-term operation. Consequently, CDs not only expand their light absorption capacity but also promote nonradiative recombination, consistently releasing thermal energy. Nevertheless, its cost-effectiveness is perceived as low at 173.21 (g h^{-1} $\$^{-1}$) in comparison to the other materials discussed.

Table 3 illustrates the synthetic sequences of investigation cases with the performance data, including the cost-effectiveness calculations.

For an overall summary, see the bullet chart in Figure 8, which connects the evaporation rate, cost, and cost-effectiveness of some solar evaporators. Each one is ordered according to evaporation rate, from low to high, demonstrating how cost-effectiveness can be balanced relative to the cost and evaporation rate. For instance, consider the mentioned example of an evaporator comprising a combination of nitrogen-doped graphene aerogel (NGA), with a normal evaporation rate of 1.497 (kg m^{-2} h^{-1}) and a low cost of $0.8 m^{-2}, resulting in high cost-effectiveness (1871.25 g h^{-1} $\$^{-1}$).[113] This configuration yielded the highest cost-effectiveness in comparison with other mentioned evaporators with different evaporation rates and material costs.

CONCLUSIONS AND OUTLOOK

Nonetheless, synthesis methods and materials cost can be optimized for further development. Through continuous refinement and innovation in synthesis techniques, researchers

https://doi.org/10.1021/acsomega.4c03040
ACS Omega 2024, 9, 27872−27887

can fine-tune both evaporation performance and material costs to complement each other, leading to even higher levels of cost-effectiveness. Additionally, exploring alternative materials and fabrication methods may yield promising results in achieving optimal performance at reduced costs. Moreover, ongoing research efforts should focus on scalability and sustainability, aiming to translate laboratory-scale achievements into practical and environmentally friendly solutions. Besides that, the accuracy of the calculation of the evaporation rate needs more development by considering the energy gained from the surrounding environment, such as natural convection.

Furthermore, there is great potential in harnessing natural resources for solar-driven evaporation systems, such as utilizing abundant sunlight and renewable materials. Researchers can explore the use of natural polymers, plant extracts, and other renewable resources as alternatives to synthetic materials, ensuring sustainability and reducing environmental impact. Additionally, the exploitation of waste materials, particularly, woods, biomass waste materials, recycled textiles, and plastics, presents an opportunity to repurpose existing resources for evaporation technology. For future work, by incorporating easily fabricated and readily available recycled materials into the design and fabrication process, researchers can further enhance the cost-effectiveness and accessibility of solar-driven evaporation systems. Moreover, it is important to explore techniques and methods for producing significant quantities of solar evaporators, such as electrodeposition or machinery-based production, aiming to strike a balance in production costs rather than depending on costly techniques limited to laboratory-scale production. Additionally, it is worth considering also the mass production of nanoparticles at low cost, which can be achieved through technologies such as high gravity reactive precipitation (HGRP). Overall, by leveraging natural resources and recycled materials, coupled with innovative fabrication techniques, the development of solar-driven evaporation technology can be accelerated, paving the way for scalable and sustainable solutions to address water scarcity challenges worldwide.

■ ASSOCIATED CONTENT

Supporting Information

The Supporting Information is available free of charge at https://pubs.acs.org/doi/10.1021/acsomega.4c03040.

More details and calculations of the cost-effectiveness are described, which also includes Table S1, illustrating more examples of cost-effective photothermal materials (PDF)

■ AUTHOR INFORMATION

Corresponding Authors

Husam Eltigani − *Metallurgy and Materials Science Research Institute (MMRI), Chulalongkorn University, Pathumwan, Bangkok 10330, Thailand*; orcid.org/0000-0003-0477-0259; Email: husamhussein.i@chula.ac.th

Yuttanant Boonyongmaneerat − *Metallurgy and Materials Science Research Institute (MMRI), Chulalongkorn University, Pathumwan, Bangkok 10330, Thailand*; Email: Yuttanant.B@chula.ac.th

Author

Viriyah Chobaomsup − *Metallurgy and Materials Science Research Institute (MMRI), Chulalongkorn University, Pathumwan, Bangkok 10330, Thailand*

Complete contact information is available at: https://pubs.acs.org/10.1021/acsomega.4c03040

Notes

The authors declare no competing financial interest.

■ ACKNOWLEDGMENTS

This work is financially supported by Rachadapisek Sompote Fund, Graduate School, Chulalongkorn University and Metallurgy and Materials Science Research Institute (MMRI), Chulalongkorn University, and Ministry of Higher Education Science Research and Innovation of Thailand (MHESI).

■ REFERENCES

(1) Arbués, F.; Garcıa-Valiñas, M.Á.; Martınez-Espiñeira, R. Estimation of residential water demand: a state-of-the-art review. *Journal of Socio-Economics* **2003**, *32* (1), 81−102.

(2) Du Plessis, A. South Africa's Water Predicament: Freshwater's Unceasing Decline. Springer Nature, 2023; Vol. *101*.

(3) Blanco, J.; et al. Review of feasible solar energy applications to water processes. *Renewable and Sustainable Energy Reviews* **2009**, *13* (6−7), 1437−1445.

(4) Alvarez, P. J.; et al. Emerging opportunities for nanotechnology to enhance water security. *Nature Nanotechnol.* **2018**, *13* (8), 634−641.

(5) Cui, X.; et al. Photothermal Nanomaterials: A Powerful Light-to-Heat Converter. *Chem. Rev.* **2023**, *123* (11), 6891−6952.

(6) Du, C.; et al. Heat-localized solar evaporation: Transport processes and applications. *Nano Energy* **2023**, *107*, 108086.

(7) Zhu, L.; Tian, L.; Jiang, S.; Han, L.; Liang, Y.; Li, Q.; Chen, S. Advances in photothermal regulation strategies: from efficient solar heating to daytime passive cooling. *Chem. Soc. Rev.* **2023**, *52*, 7389.

(8) Ge, Y.; et al. Self-rotating spherical evaporator based on hydrogel and black titanium oxide for continuous desalination of seawater. *ACS Materials Letters* **2023**, *5* (9), 2576−2583.

(9) Wang, J.; et al. In situ polymerized Fe2O3@ PPy/chitosan hydrogels as a hydratable skeleton for solar-driven evaporation. *J. Am. Ceram. Soc.* **2022**, *105* (8), 5325−5335.

(10) Cheng, P.; et al. Advanced phase change hydrogel integrating metal-organic framework for self-powered thermal management. *Nano Energy* **2023**, *105*, 108009.

(11) Zhou, S.; Kong, X.; Strømme, M.; Xu, C. Efficient Solar Thermal Energy Conversion and Utilization by a Film of Conductive Metal−Organic Framework Layered on Nanocellulose. *ACS Materials Letters* **2022**, *4* (6), 1058−1064.

(12) Song, Z.; Ge, C.; Song, Y.; Chen, Z.; Shao, B.; Yuan, X.; Chen, J.; Xu, D.; Song, T.; Fang, J.; Wang, Y.; Sun, B. Synergistic Solar-Driven Freshwater Generation and Electricity Output Empowered by Wafer-Scale Nanostructured Silicon. *Small* **2023**, *19* (4), 2205265.

(13) Kim, J.; et al. Scalable high-efficiency bi-facial solar evaporator with a dendritic copper oxide wick. *ACS Appl. Mater. Interfaces* **2021**, *13* (10), 11869−11878.

(14) Verma, N. C.; Yadav, A.; Nandi, C. K. Paving the path to the future of carbogenic nanodots. *Nat. Commun.* **2019**, *10* (1), 2391.

(15) Hu, S.; Qin, L.; Yi, H.; Lai, C.; Yang, Y.; Li, B.; Fu, Y.; Zhang, M.; Zhou, X. Carbonaceous Materials-Based Photothermal Process in Water Treatment: From Originals to Frontier Applications. *Small* **2024**, *20* (5), 2305579.

(16) Ghosal, S.; Mondal, N. S.; Chowdhury, S.; Jana, D. Two novel phases of germa-graphene: Prediction, electronic and transport applications. *Appl. Surf. Sci.* **2023**, *614*, 156107.

(17) Linic, S.; Chavez, S.; Elias, R. Flow and extraction of energy and charge carriers in hybrid plasmonic nanostructures. *Nat. Mater.* **2021**, *20* (7), 916−924.
(18) Dahliah, D.; et al. High-throughput computational search for high carrier lifetime, defect-tolerant solar absorbers. *Energy Environ. Sci.* **2021**, *14* (9), 5057−5073.
(19) Liu, H.; et al. Development of renewable biomass-derived carbonaceous aerogel/mannitol phase-change composites for high thermal-energy-release efficiency and shape stabilization. *ACS Applied Energy Materials* **2021**, *4* (2), 1714−1730.
(20) Liu, Z.; et al. High-absorption recyclable photothermal membranes used in a bionic system for high-efficiency solar desalination: Via enhanced localized heating. *Journal of Materials Chemistry A* **2017**, *5* (37), 20044−20052.
(21) Huang, Q.; Du, C.; Huang, C. Nature-inspired pyramid-shaped 3-dimensional structure for cost-effective heat-localized solar evaporation with high efficiency and salt localization. *Applied Thermal Engineering* **2022**, *215*, 118950.
(22) Asghar, M. S.; Arshad, N.; Tao, J.; Irshad, M. S.; Li, J.; Wang, X. Recent Advances in Multifunctional Photothermal Materials for Solar-Driven Steam and Energy Generation. *Energy Technology* **2023**, *11* (9), 2300500.
(23) Hazra, S. K.; Saleque, A. M.; Thakur, A. K.; Ivan, M. N. A. S.; Biswas, D.; Khan, S. A.; Saidur, R.; Ma, Z.; Sathyamurthy, R. Recent Advancement in Solar-Driven Interfacial Steam Generation for Desalination: A State-of-the-Art Review. *Energy Technology* **2024**, *12*, 2301190.
(24) Xu, X.; Garemark, J.; Ram, F.; Wang, Z.; Li, Y. Metallic Wood through Deep-Cell-Wall Metallization: Synthesis and Applications. *ACS Appl. Mater. Interfaces* **2024**, *16*, 22433.
(25) Wang, Y.; Liu, X.; Zhang, Q.; Wang, C.; Huang, S.; Liu, Y.; Yu, T.; Yang, R.; Chen, G.; Chaker, M.; Ma, D. Stable, Cost-Effective TiN-Based Plasmonic Nanocomposites with over 99% Solar Steam Generation Efficiency. *Adv. Funct. Mater.* **2023**, *33* (15), 2212301.
(26) Ku, B.-J.; et al. Solar-driven desalination using salt-rejecting plasmonic cellulose nanofiber membrane. *J. Colloid Interface Sci.* **2023**, *634*, 543−552.
(27) Zhu, L.; Gao, M.; Peh, C. K. N.; Ho, G. W. Solar-driven photothermal nanostructured materials designs and prerequisites for evaporation and catalysis applications. *Materials Horizons* **2018**, *5* (3), 323−343.
(28) Jiang, H.; Liu, X.; Wang, D.; Qiao, Z.; Wang, D.; Huang, F.; Peng, H.; Hu, C. Designing high-efficiency light-to-thermal conversion materials for solar desalination and photothermal catalysis. *Journal of Energy Chemistry* **2023**, *79*, 581.
(29) Chen, C.; Kuang, Y.; Hu, L. Challenges and Opportunities for Solar Evaporation. *Joule* **2019**, *3* (3), 683−718.
(30) Zhang, Y.; Xiong, T.; Nandakumar, D. K.; Tan, S. C. Structure architecting for salt-rejecting solar interfacial desalination to achieve high-performance evaporation with in situ energy generation. *Advanced Science* **2020**, *7* (9), 1903478.
(31) Ni, G.; Li, G.; Boriskina, S. V.; Li, H.; Yang, W.; Zhang, T.; Chen, G. Steam generation under one sun enabled by a floating structure with thermal concentration. *Nature Energy* **2016**, *1* (9), 16126 DOI: 10.1038/nenergy.2016.126.
(32) Ghasemi, H.; Ni, G.; Marconnet, A. M.; Loomis, J.; Yerci, S.; Miljkovic, N.; Chen, G. Solar steam generation by heat localization. *Nat. Commun.* **2014**, *5*, 4449 DOI: 10.1038/ncomms5449.
(33) Tian, Y.; Song, R.; Li, Y.; Zhu, R.; Yang, X.; Wu, D.; Wang, X.; Song, J.; Yu, J.; Gao, T.; Li, F. Biomimetic Structural Design of Fabric for Low-Cost, Scalable, and Highly Efficient Off-Grid Solar-Driven Water Purification. *Adv. Funct. Mater.* **2024**, *34*, 2309470.
(34) Chen, Y.-Z.; Yang, H.-C.; Li, H.-N.; Xin, J.-H.; Zhang, C.; Wan, L.-S.; Xu, Z.-K.; et al. Self-Flipping Solar Seesaw Evaporators Leverage Scaling to De-Scale. *Small* **2024**, 2310952.
(35) Zhang, P.; Wang, H.; Wang, J.; Ji, Z.; Qu, L. Boosting the Viable Water Harvesting in Solar Vapor Generation: From Interfacial Engineering to Devices Design. *Adv. Mater.* **2024**, *36*, 2303976.
(36) Liu, S.; Wang, X.; Chen, Y.; Li, Y.; Wei, Y.; Shao, T.; Ma, J.; Jiang, W.; Xu, J.; Dong, Y.; Wang, C.; Liu, H.; Gao, C.; Xiong, Y. Efficient Thermal Management with Selective Metamaterial Absorber for Boosting Photothermal CO2 Hydrogenation under Sunlight. *Adv. Mater.* **2024**, *36*, 2311957.
(37) Hu, H.; et al. Ultra-broadband perfect absorber based on self-organizing multi-scale plasmonic nanostructures. *Applied Materials Today* **2022**, *26*, 101266.
(38) Tang, R.; Ju, J.; Huang, Y.; Kang, W. A review: Electrospinning applied to solar interfacial evaporator. *Solar RRL* **2023**, *7* (20), 2300382.
(39) Fan, Q.; et al. The role of micro-nano pores in interfacial solar evaporation systems−a review. *Applied Energy* **2021**, *292*, 116871.
(40) Xu, Z.; et al. Ultrahigh-efficiency desalination via a thermally-localized multistage solar still. *Energy Environ. Sci.* **2020**, *13* (3), 830−839.
(41) Chen, C.; et al. Dendritic Structure-Inspired Coating Strategy for Stable and Efficient Solar Evaporation of Salinity Brine. *ACS Sustainable Chem. Eng.* **2023**, *11* (9), 3882−3895.
(42) Luo, Y.-Q.; et al. Advanced solar desalination on superwetting surfaces. *Journal of Materials Chemistry A* **2022**, *10* (37), 19348−19366.
(43) Abdelsalam, M. A.; Sajjad, M.; Raza, A.; AlMarzooqi, F.; Zhang, T. Sustainable biomimetic solar distillation with edge crystallization for passive salt collection and zero brine discharge. *Nat. Commun.* **2024**, *15* (1), 874.
(44) Wilson, H. M.; Rahman, S. A. R.; Parab, A. E.; Jha, N. Ultra-low cost cotton based solar evaporation device for seawater desalination and waste water purification to produce drinkable water. *Desalination* **2019**, *456*, 85−96.
(45) Xu, N.; Li, J.; Finnerty, C.; Song, Y.; Zhou, L.; Zhu, B.; Wang, P.; Mi, B.; Zhu, J. Going beyond efficiency for solar evaporation. *Nature Water* **2023**, *1*, 494.
(46) Wang, Y.; et al. Ti3C2T x MXene Nanoflakes Embedded with Copper Indium Selenide Nanoparticles for Desalination and Water Purification through High-Efficiency Solar-Driven Membrane Evaporation. *ACS Appl. Mater. Interfaces* **2022**, *14* (4), 5876−5886.
(47) He, F.; et al. A simple, mild and versatile method for preparation of photothermal woods toward highly efficient solar steam generation. *Nano Energy* **2020**, *71*, 104650.
(48) Metyouy, K.; et al. Hydrothermal carbonization vs. anaerobic digestion to valorize fruit and vegetable waste: A comparative technical and energy assessment. *Journal of Environmental Chemical Engineering* **2023**, *11* (3), 109925.
(49) Iranshahi, K.; et al. Electrohydrodynamic drying versus conventional drying methods: A comparison of key performance indicators. *Energy Conversion and Management* **2023**, *279*, 116661.
(50) Ipiales, R. P.; Pimentel-Betancurt, D.; Diaz, E.; de la Rubia, A.; Rodriguez, J. J.; Mohedano, A. F. Energy Recovery from Garden and Park Waste by Hydrothermal Carbonization with Process Water Recycling. *ACS Sustainable Chem. Eng.* **2024**, *12*, 5229.
(51) Javed, M.; et al. Complete system to generate clean water from a contaminated water body by a handmade flower-like light absorber. *ACS omega* **2021**, *6* (50), 35104−35111.
(52) Berglund, J.; Mikkelsen, D.; Flanagan, B. M.; Dhital, S.; Gaunitz, S.; Henriksson, G.; Lindstrom, M. E.; Yakubov, G. E.; Gidley, M. J.; Vilaplana, F. Wood hemicelluloses exert distinct biomechanical contributions to cellulose fibrillar networks. *Nat. Commun.* **2020**, *11* (1), 4692.
(53) Chen, C.; et al. Structure−property−function relationships of natural and engineered wood. *Nature Reviews Materials* **2020**, *5* (9), 642−666.
(54) Kim, K.; et al. Mesoporous three-dimensional graphene networks for highly efficient solar desalination under 1 sun illumination. *ACS Appl. Mater. Interfaces* **2018**, *10* (18), 15602−15608.
(55) Jiang, F.; Li, T.; Li, Y.; Zhang, Y.; Gong, A.; Dai, J.; Hitz, E.; Luo, W.; Hu, L. Wood-based nanotechnologies toward sustainability. *Adv. Mater.* **2018**, *30* (1), 1703453.

https://doi.org/10.1021/acsomega.4c03040
ACS Omega 2024, 9, 27872−27887

(56) Zhao, F.; et al. Materials for solar-powered water evaporation. *Nature Reviews Materials* **2020**, *5* (5), 388−401.
(57) Kuang, Y.; Chen, C.; He, S.; Hitz, E. M.; Wang, Y.; Gan, W.; Mi, R.; Hu, L. A high-performance self-regenerating solar evaporator for continuous water desalination. *Advanced materials* **2019**, *31* (23), 1900498.
(58) Li, T.; Liu, H.; Zhao, X.; Chen, G.; Dai, J.; Pastel, G.; Jia, C.; Chen, C.; Hitz, E.; Siddhartha, D.; Yang, R.; Hu, L. Scalable and highly efficient mesoporous wood-based solar steam generation device: localized heat, rapid water transport. *Adv. Funct. Mater.* **2018**, *28* (16), 1707134.
(59) Wei, D.; Wang, C.; Zhang, J.; Zhao, H.; Asakura, Y.; Eguchi, M.; Xu, X.; Yamauchi, Y. Water Activation in Solar-Powered Vapor Generation. *Adv. Mater.* **2023**, *35* (47), 2212100.
(60) Jia, C.; et al. Rich mesostructures derived from natural woods for solar steam generation. *Joule* **2017**, *1* (3), 588−599.
(61) Cui, T.; et al. Engineered wood with hierarchically tunable microchannels toward efficient solar vapor generation. *Langmuir* **2022**, *38* (42), 12773−12784.
(62) Lai, K. C.; et al. Environmental application of three-dimensional graphene materials as adsorbents for dyes and heavy metals: Review on ice-templating method and adsorption mechanisms. *Journal of Environmental Sciences* **2019**, *79*, 174−199.
(63) Li, M.; Dai, X.; Gao, W.; Bai, H. Ice-templated fabrication of porous materials with bioinspired architecture and functionality. *Accounts of Materials Research* **2022**, *3* (11), 1173−1185.
(64) Ghafurian, M. M.; Niazmand, H.; Ebrahimnia-Bajestan, E.; Taylor, R. A. Wood surface treatment techniques for enhanced solar steam generation. *Renewable Energy* **2020**, *146*, 2308−2315.
(65) Yu, Z.; et al. Enhancing efficiency of carbonized wood based solar steam generator for wastewater treatment by optimizing the thickness. *Sol. Energy* **2019**, *193*, 434−441.
(66) Xie, M.; Zhang, P.; Cao, Y.; Yan, Y.; Wang, Z.; Jin, C. A three-dimensional antifungal wooden cone evaporator for highly efficient solar steam generation. *npj Clean Water* **2023**, *6* (1), 12.
(67) Zhang, X.; et al. Nature-inspired design: p-toluenesulfonic acid-assisted hydrothermally engineered wood for solar steam generation. *Nano Energy* **2020**, *78*, 105322.
(68) Zhang, H.; et al. Highly thermally insulated and super-hydrophilic corn straw for efficient solar vapor generation. *ACS Appl. Mater. Interfaces* **2020**, *12* (14), 16503−16511.
(69) Zhu, M.; Li, Y.; Chen, G.; Jiang, F.; Yang, Z.; Luo, X.; Wang, Y.; Lacey, S. D.; Dai, J.; Wang, C.; Jia, C.; Wan, J.; Yao, Y.; Gong, A.; Yang, B.; Yu, Z.; Das, S.; Hu, L. Tree-inspired design for high-efficiency water extraction. *Adv. Mater.* **2017**, *29* (44), 1704107.
(70) Liu, J.; Yao, J.; Yuan, Y.; Liu, Q.; Zhang, W.; Zhang, X.; Gu, J. Surface-carbonized bamboos with multilevel functional biostructures deliver high photothermal water evaporation performance. *Advanced Sustainable Systems* **2020**, *4* (9), 2000126.
(71) Feng, Q.; et al. An efficient torrefaction Bamboo-based evaporator in interfacial solar steam generation. *Sol. Energy* **2021**, *230*, 1095−1105.
(72) Chen, Y.; et al. Bamboo shoot-based evaporator with self-cleaning and mildew-resistant for efficient solar steam generation. *Desalination* **2022**, *541*, 116003.
(73) Li, Z.; Wang, C.; Lei, T.; Ma, H.; Su, J.; Ling, S.; Wang, W. Arched bamboo charcoal as interfacial solar steam generation integrative device with enhanced water purification capacity. *Advanced Sustainable Systems* **2019**, *3* (4), 1800144.
(74) Atinafu, D. G.; Kim, Y. U.; Kim, S.; Kang, Y.; Kim, S. Advances in biocarbon and soft material assembly for enthalpy storage: Fundamentals, mechanisms, and multimodal applications. *Small* **2024**, *20* (13), 2305418.
(75) Ovando-Medina, V. M.; Escobar-Villanueva, A. G.; Martínez-Gutiérrez, H.; González-Ortega, O. Interfacial photothermal water evaporator based on nanoporous microwave-expanded graphite and coconut waste fibers@ recycled polystyrene as substrate. *International Journal of Energy Research* **2020**, *44* (13), 10878−10893.
(76) Zhang, B.; Fan, C.; Guo, W.; Zhu, Y. Cryptomelane Modified Biomass Wastes for Solar Interfacial Evaporation and Stabilization of Cadmium. *Water, Air, & Soil Pollution* **2023**, *234* (5), 1−15.
(77) Zhu, M.; et al. Carbonized daikon for high efficient solar steam generation. *Sol. Energy Mater. Sol. Cells* **2019**, *191*, 83−90.
(78) Xu, N. Mushrooms as efficient solar steam-generation devices. *Adv. Mater.* **2017**, *29* (28), 1606762.
(79) Liu, C.; et al. Biomass-based high-efficiency solar-driven interface evaporator based on natural pomelo peel with multi-curvature gradient structure. *Colloids Surf., A* **2023**, *674*, 131969.
(80) Fang, S.; Lyu, X.; Tong, T.; Lim, A. I.; Li, T.; Bao, J.; Hu, Y. H.; et al. Turning dead leaves into an active multifunctional material as evaporator, photocatalyst, and Bioplastic. *Nat. Commun.* **2023**, *14* (1), 1203.
(81) Cao, S.; Rathi, P.; Wu, X.; Ghim, D.; Jun, Y.-S.; Singamaneni, S.; et al. Cellulose nanomaterials in interfacial evaporators for desalination: a "natural" choice. *Adv. Mater.* **2021**, *33* (28), 2000922.
(82) Khajevand, M.; Azizian, S.; Boukherroub, R. Naturally abundant green moss for highly efficient solar thermal generation of clean water. *ACS Appl. Mater. Interfaces* **2021**, *13* (27), 31680−31690.
(83) Luo, B.; Wen, J.; Wang, H.; Zheng, S.; Liao, R.; Chen, W.; Mahian, O.; Li, X. A Biomass-Based Hydrogel Evaporator Modified Through Dynamic Regulation of Water Molecules: Highly Efficient and Cost-Effective. *Energy and Environmental Materials* **2023**, *6* (3), No. e12353.
(84) Gao, S.; Dong, X.; Huang, J.; Dong, J.; Maggio, F. D.; Wang, S.; Guo, F.; Zhu, T.; Chen, Z.; Lai, Y. Bioinspired soot-deposited Janus fabrics for sustainable solar steam generation with salt-rejection. *Global Challenges* **2019**, *3* (8), 1800117.
(85) Gao, C.; et al. Reversed vapor generation with Janus fabric evaporator and comprehensive thermal management for efficient interfacial solar distillation. *Chemical Engineering Journal* **2023**, *463*, 142002.
(86) Wang, W.; et al. Full cattail leaf-based solar evaporator with square water transport channels for cost-effective solar vapor production. *Cellulose* **2023**, *30* (2), 1103−1115.
(87) Yang, Y.; et al. Low-cost and scalable carbon bread used as an efficient solar steam generator with high performance for water desalination and purification. *RSC Adv.* **2021**, *11* (15), 8674−8681.
(88) Eriksen, M.; et al. A growing plastic smog, now estimated to be over 170 trillion plastic particles afloat in the world's oceans—Urgent solutions required. *PLoS One* **2023**, *18* (3), No. e0281596.
(89) Moharir, R. V.; Kumar, S. Challenges associated with plastic waste disposal and allied microbial routes for its effective degradation: A comprehensive review. *Journal of Cleaner Production* **2019**, *208*, 65−76.
(90) Kim, S.; Bowen, R. A.; Zare, R. N. Transforming plastic surfaces with electrophilic backbones from hydrophobic to hydrophilic. *ACS Appl. Mater. Interfaces* **2015**, *7* (3), 1925−1931.
(91) Sun, H.; et al. Facile preparation of a carbon-based hybrid film for efficient solar-driven interfacial water evaporation. *ACS Appl. Mater. Interfaces* **2021**, *13* (28), 33427−33436.
(92) Han, S.-J.; Xu, L.; Liu, P.; Wu, J.-L.; Labiadh, L.; Fu, M.-L.; Yuan, B. Recycling Graphite from Spent Lithium Batteries for Efficient Solar-Driven Interfacial Evaporation to Obtain Clean Water. *ChemSusChem* **2023**, *16*, No. e202300845.
(93) Li, X.; et al. Efficiency enhancement on the solar steam generation by wick materials with wrapped graphene nanoparticles. *Applied Thermal Engineering* **2019**, *161*, 114195.
(94) Zhang, Y.; et al. Robust, scalable, and cost-effective surface carbonized pulp foam for highly efficient solar steam generation. *ACS Appl. Mater. Interfaces* **2023**, *15* (5), 7414−7426.
(95) Wang, J.; Shi, Q.; Li, C.; Zhang, Y.; Du, S.; Mao, J.; Wang, J. Pistia-inspired photothermal fabric based on waste carbon fiber for low-cost vapor generation: an industrialization route. *Adv. Funct. Mater.* **2022**, *32* (26), 2201922.
(96) Li, Y.; Wang, R.; Zhang, L.; Wang, X.; Zhang, K.; Shou, W.; Fan, J. Scalable Fabric-Based Solar Steam Generator. *Adv. Funct. Mater.* **2024**, *34*, 2312613.

https://doi.org/10.1021/acsomega.4c03040
ACS Omega 2024, 9, 27872−27887

(97) Kospa, D. A.; et al. Flexible CuO-rGO/PANI thermal absorber with high broadband photoresponse and salt resistance for efficient desalination of oil-contaminated seawater. *Desalination* **2022**, *528*, 115612.
(98) Gong, B.; et al. Phase change material enhanced sustained and energy-efficient solar-thermal water desalination. *Applied Energy* **2021**, *301*, 117463.
(99) Liu, F.; Zhao, B.; Wu, W.; Yang, H.; Ning, Y.; Lai, Y.; Bradley, R. Low cost, robust, environmentally friendly geopolymer–mesoporous carbon composites for efficient solar powered steam generation. *Adv. Funct. Mater.* **2018**, *28* (47), 1803266.
(100) Lin, X.; et al. Integrative solar absorbers for highly efficient solar steam generation. *Journal of Materials Chemistry A* **2018**, *6* (11), 4642–4648.
(101) Kazi, O. A.; Chen, W.; Eatman, J. G.; Gao, F.; Liu, Y.; Wang, Y.; Xia, Z.; Darling, S. B. Material design strategies for recovery of critical resources from water. *Adv. Mater.* **2023**, *35* (36), 2300913.
(102) Rastgar, M.; Jiang, L.; Wang, C.; Sadrzadeh, M. Aerogels in passive solar thermal desalination: a review. *Journal of Materials Chemistry A* **2022**, *10* (35), 17857–17877.
(103) Zhao, Q.; et al. Integrated strategy of solar evaporator and steam collector configurations for interfacial evaporation water purification. *Sol. Energy* **2023**, *266*, 112187.
(104) Gao, J.; et al. A simple and controllable black hydrogel coating strategy to prepare self-cleaning and durable evaporator for efficient solar steam generation. *Desalination* **2023**, *549*, 116341.
(105) Jeon, J.; Lee, S. H.; Lee, S.-R.; Seo, T. H.; Kim, Y.-K. Biorenewable Polymer-Based Light-Absorbing Porous Hydrogel for Efficient Solar Steam Desalination. *ACS Appl. Mater. Interfaces* **2023**, *15*, 30692.
(106) Wang, M.; et al. Hierarchically structured bilayer Aerogel-based Salt-resistant solar interfacial evaporator for highly efficient seawater desalination. *Sep. Purif. Technol.* **2022**, *287*, 120534.
(107) Zhang, H.; et al. Biomimetic hydrogel with directional heat regulation for efficient solar desalination. *Chemical Engineering Journal* **2023**, *473*, 145484.
(108) Li, N.; et al. Shape-controlled fabrication of cost-effective, scalable and anti-biofouling hydrogel foams for solar-powered clean water production. *Chemical Engineering Journal* **2022**, *431*, 134144.
(109) Guo, Y.; Lu, H.; Zhao, F.; Zhou, X.; Shi, W.; Yu, G. Biomass-derived hybrid hydrogel evaporators for cost-effective solar water purification. *Advanced materials* **2020**, *32* (11), 1907061.
(110) Meng, X.; et al. A biomass-derived, all-day-round solar evaporation platform for harvesting clean water from microplastic pollution. *Journal of Materials Chemistry A* **2021**, *9* (17), 11013–11024.
(111) Li, Y.; Shi, Y.; Wang, H.; Liu, T.; Zheng, X.; Gao, S.; Lu, J. Recent advances in carbon-based materials for solar-driven interfacial photothermal conversion water evaporation: Assemblies, structures, applications, and prospective. *Carbon Energy* **2023**, *5*, No. e331.
(112) Du, R.; et al. Coupling ultrafine plasmonic Co3O4 with thin-layer carbon over SiO2 nanosphere for dual-functional PMS activation and solar interfacial water evaporation. *J. Alloys Compd.* **2023**, *940*, 168816.
(113) Deng, X.; et al. Nitrogen-doped unusually superwetting, thermally insulating, and elastic graphene aerogel for efficient solar steam generation. *ACS Appl. Mater. Interfaces* **2020**, *12* (23), 26200–26212.
(114) Yin, M.; Hsin, Y.; Guo, X.; Zhang, R.; Huang, X.; Zhang, X. Facile and low-cost ceramic fiber-based carbon-carbon composite for solar evaporation. *Sci. Total Environ.* **2021**, *759*, 143546.
(115) Nguyen, U. N. T.; et al. Shape-transformable long-lasting superhydrophilic carbon cloth for sustainable solar vapor generation. *Chemical Engineering Journal* **2024**, *481*, 148475.
(116) Li, J.; Yu, F.; Jiang, Y.; Wang, L.; Yang, X.; Li, X.; Lu, W.; Sun, X. Photothermal Diatomite/Carbon Nanotube Combined Aerogel for High-Efficiency Solar Steam Generation and Wastewater Purification. *Solar RRL* **2022**, *6* (4), 2101011.
(117) Monavari, S. M.; Marsusi, F.; Memarian, N.; Qasemnazhand, M. Carbon nanotubes and nanobelts as potential materials for biosensor. *Sci. Rep.* **2023**, *13* (1), 3118.
(118) Lv, S.; et al. Preparation and performance study of scalable high-efficiency solar steam generated system. *Applied Thermal Engineering* **2023**, *229*, 120597.
(119) Zhao, D.; Ding, M.; Lin, T.; Duan, Z.; Wei, R.; Feng, P.; Yu, J.; Liu, C.-Y.; Li, C. Gradient Graphene Spiral Sponges for Efficient Solar Evaporation and Zero Liquid Discharge Desalination with Directional Salt Crystallization. *Advanced Science* **2024**, *11*, 2400310.
(120) Zhou, H.; et al. Assembling carbon dots on vertically aligned acetate fibers as ideal salt-rejecting evaporators for solar water purification. *Chemical Engineering Journal* **2021**, *421*, 129822.
(121) Yin, M.; et al. Facile and low-cost ceramic fiber-based carbon-carbon composite for solar evaporation. *Science of The Total Environment* **2021**, *759*, 143546.
(122) Zhou, H.; Xue, C.; Chang, Q.; Yang, J.; Hu, S. Assembling carbon dots on vertically aligned acetate fibers as ideal salt-rejecting evaporators for solar water purification. *Chemical Engineering Journal* **2021**, *421*, 129822.
(123) Meng, X.; et al. Full-colour carbon dots: from energy-efficient synthesis to concentration-dependent photoluminescence properties. *Chem. Commun.* **2017**, *53* (21), 3074–3077.
(124) Cheng, S.; Liu, C.; Li, Y.; Tan, H.; Wang, Y.; Li, Y. Polyoxometalates-Modulated Hydrophilic-Hydrophobic Composite Interfacial Material for Efficient Solar Water Evaporation and Salt Harvesting in High-Salinity Brine. *Energy & Environmental Materials* **2024**, *7*, No. e12647.
(125) Zhao, Q.; et al. Superwetting B4C bilayer foam for high cost-performance solar water purification. *Materials Today Energy* **2020**, *18*, 100498.
(126) Wang, Z.; et al. Porifera-inspired cost-effective and scalable "porous hydrogel sponge" for durable and highly efficient solar-driven desalination. *Chemical Engineering Journal* **2022**, *427*, 130905.
(127) Luo, B.; Wen, J.; Wang, H.; Zheng, S.; Liao, R.; Chen, W.; Mahian, O.; Li, X.; et al. A biomass-based hydrogel evaporator modified through dynamic regulation of water molecules: highly efficient and cost-effective. *Energy & Environmental Materials* **2023**, *6* (3), No. e12353.
(128) Wu, T.; et al. Scalable and cost-effective fabrication of self-floating three-dimensional interconnected polyethylene/multiwall carbon nanotubes composite foam for high evaporation performance. *Composites Part B: Engineering* **2022**, *243*, 110111.
(129) Zhu, Y.; Tian, G.; Liu, Y.; Li, H.; Zhang, P.; Zhan, L.; Gao, R.; Huang, C.; et al. Low-cost, unsinkable, and highly efficient solar evaporators based on coating MWCNTs on nonwovens with unidirectional water-transfer. *Advanced Science* **2021**, *8* (19), 2101727.
(130) Xu, Y.; et al. Easily scaled-up photo-thermal membrane with structure-dependent auto-cleaning feature for high-efficient solar desalination. *J. Membr. Sci.* **2019**, *586*, 222–230.
(131) Xiong, J.; et al. Hierarchical MnO2 nanosheets grown on cotton fabric as a flexible and washable solar evaporator for seawater desalination. *ACS Applied Nano Materials* **2021**, *4* (12), 13724–13733.
(132) Lu, X.; et al. Hyperstable and compressible plant fibers/chitosan aerogel as portable solar evaporator. *Sol. Energy* **2022**, *231*, 828–836.
(133) Zhong, X.; et al. Turnover polypyrrole decorated cotton fabric based solar evaporator for cost-effective and steady desalination. *Journal of Cleaner Production* **2023**, *417*, 138088.

https://doi.org/10.1021/acsomega.4c03040
ACS Omega 2024, 9, 27872–27887